HIGH FREQUENCY ULTRASOUND TRANSDUCER FOR REAL TIME ULTRASOUND BIOMICROSCOPY WITH OPTOACOUSTIC ARRAYS

by

Xinqing Guo

A thesis submitted to the Faculty of the University of Delaware in partial fulfillment of the requirements for the degree of Master of Science in Electrical and Computer Engineering

Spring 2011

HIGH FREQUENCY ULTRASOUND TRANSDUCER

FOR REAL TIME ULTRASOUND BIOMICROSCOPY

WITH OPTOACOUSTIC ARRAYS

by

Xinqing Guo

Approved: _____

Takashi Buma, Ph.D.
Professor in charge of thesis on behalf of the Advisory Committee

Approved: _____

Kenneth E. Barner, Ph.D.
Chair of the Department of Electrical and Computer Engineering

Approved: _____

Michael J. Chajes, Ph.D.
Dean of the College of Engineering

Approved: _____

Charles G. Riordan, Ph.D.
Vice Provost for Graduate and Professional Education

ACKNOWLEDGMENTS

Foremost, I would like to express my sincere gratitude to my advisor Prof. Takashi Buma for his guidance during my research and study. His attitude and enthusiasm in teaching and research had motived all his students, including me. He was always accessible and willing to help his students with their research. I could not have imaged having a better advisor and mentor for my graduate study.

Besides my advisor, I wish to express my warm and sincere thanks to Prof. Sylvain Cloutier, Prof. Keith Goossen and Prof. Dennis Prather for their insightful comments and support to my research.

All my lab buddies at Optics and Ultrasonics Laboratory made it a comfort place to work. I would like to thank Ya Shu, Mengyang Liu and Zhuopeng Zhang, for the joy we share and the fun we have in last three years. Also, I want to thank my "coordinator", Jian Bai and Liang Qiu, for all their advice and constant support on my research.

Last but not least, I want to thank my parents and my girlfriend, Yusu. Without their encouragement and understanding, it would be impossible for me to finish this work. Thank you for always be with me and support me.

TABLE OF CONTENTS

LIST OF TABLES

LIST OF FIGURES

ABSTRACT

Ultrasound biomicroscopy (UBM) is a high resolution biomedical imaging technique using high frequency ultrasound waves. Fabricating highly populated detector arrays represents a major technical challenge for real-time UBM systems. A potential solution is optoacoustic technology, where high frequency ultrasound is detected with optical methods. The advantages of optoacoustic detection are large bandwidth, good sensitivity, and the capability for large scale parallel read-out. In this thesis, the receiving and transmitting part of a UBM imaging array are investigated separately. Optoacoustic detection is explored with a thin film etalon consisting of two gold films separated by a transparent layer. Simulations and experiments demonstrate that optoacoustic detection sensitivity is maximized with a gold layer thickness of 45 nm. Various transparent layer materials were investigated, including polystyrene microspheres, SU-8 2005 photoresist, and parylene. Experiments demonstrate that parylene is the best material due to its precise thickness control and uniformity. Ideally, the ultrasound transmitter and optoacoustic etalon are integrated into a single device. Piezoelectric materials are the most efficient emitters of ultrasound, but optical transparency is required to facilitate integration with an etalon. Lithium niobate ($LiNbO_3$) is chosen for its high piezoelectricity and excellent optical transparency. Initial efforts with $LiNbO_3$ concentrated on fabricating a

"conventional" transducer that is not optically transparent. An unfocused transducer was fabricated that produces 25 MHz ultrasound with a -6 dB bandwidth of 15 MHz and a two-way insertion loss of 27.6 dB. An optically transparent $LiNbO_3$ transducer with indium tin oxide (ITO) electrodes is currently under development. An approach to combine the optically transparent $LiNbO_3$ emitter with an optoacoustic etalon is proposed.

Chapter 1

INTRODUCTION TO ULTRASOUND BIOMICROSCOPY

Ultrasound imaging technology has been widely used for decades due to its low cost and non-invasive feature. Currently higher resolution of ultrasound imaging is developed for clinical use and small animal imaging. In this chapter we will briefly introduce the ultrasound imaging, optoacoustic imaging and ultrasound biomicroscopy.

1.1 Ultrasound Imaging

Ultrasonic imaging is an ultrasound-based diagnostic imaging technique used for visualizing subcutaneous body structures. In physics, ultrasound is sound with frequencies higher than the highest frequency that can be heard by human beings, which means that any sound above about 20 KHz is considered to be ultrasound. However, in actual applications, medical ultrasound systems operate at much higher frequencies than this defining frequency, typically between 1 and 10 MHz.

Ultrasound imaging is fundamentally an echo ranging technique. An ultrasound transducer, which converts electrical signal to acoustic signal, emits an ultrasound pulse into the body and listens for echoes reflected off tissue structure. Ultrasound wave speed depends on the material through which they are travelling. The strength and arrival time of these echoes are used to reconstruct the reflectivity and position of the tissue structure.

The major advantage of ultrasound imaging is noninvasive, which is usually painless for patient. And moreover, unlike X-ray imaging, ultrasound imaging uses no ionizing radiation, thus pose no health risk to human being. Also, ultrasound imaging is a real-time imaging technique; it is among the least expensive medical imaging systems and is portable. All these factors determine that ultrasound imaging is the most widely used medical imaging system in the world.

1.2 Ultrasound Biomicroscopy (UBM)

As mentioned above, conventional ultrasound scanners typically employ ultrasonic frequencies between 1 and 10 MHz, which corresponds to wavelengths greater than 150 μm in tissue. Higher resolution images require smaller ultrasonic wavelengths, and therefore higher frequencies. UBM systems use ultrasonic frequencies above 50 MHz. This regime of ultrasound imaging is called ultrasound biomicroscopy (UBM). Like conventional ultrasound system, UBM can help us to visualize extremely small physiological structures in living tissue in a noninvasive manner.

1.3 Clinical Significance of UBM

Due to the frequency dependent attenuation of tissue, clinical application of UBM involves superficial organs such as the skin and cornea. However, this by no means restricts the significance of UBM. In the United States, more than one million new cases of skin cancer, and over 50,000 melanoma cases, arise every year [1]. Over two million Americans have glaucoma, a leading cause of blindness due to excessive fluid pressure in the anterior segment of the eye [2]. Accurate visualization of the skin and anterior segment of the eye play a vital role in comprehensive clinical

examinations, early diagnosis, and more efficient patient care. Therefore, it is highly attractive for patients to have noninvasive real-time in vivo exams. The long term goal is to make UBM a standard part of the clinician's toolbox of high resolution imaging modalities.

UBM systems provide exquisite "B-mode" images, which are cross-sectional images where the vertical axis is depth and the horizontal axis is lateral distance. Fig.1.1 shows a B-mode image of the anterior segment of a human eye [3].

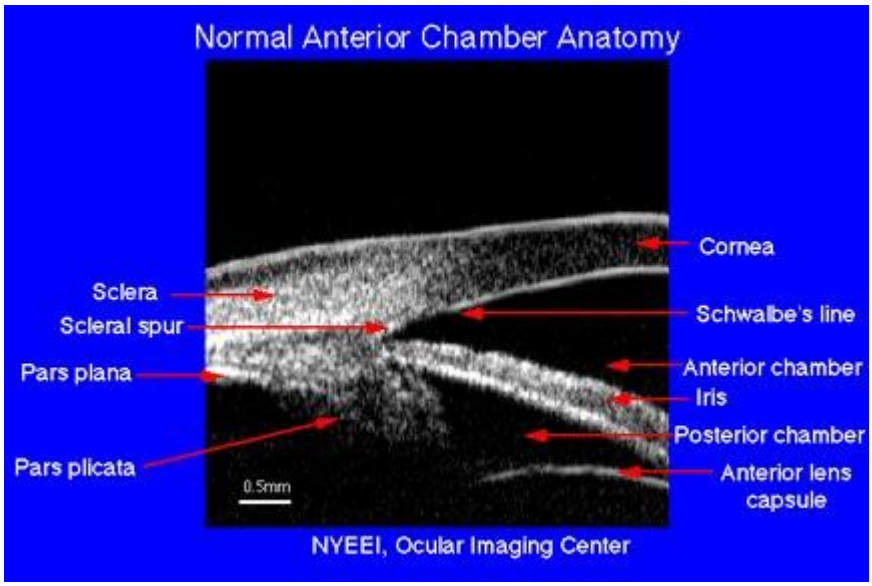

Figure 1.1 B-mode image of the anterior segment of a human eye

In UBM image, portions of the cornea, iris, and sclera can be clearly seen. This level of spatial resolution, which cannot be achieved using conventional ultrasound image, is essential for detecting early stage disease and monitoring subtle changes in developing embryos inside mice.

Another major application of UBM is small animal imaging. Mice are the preferred models for genetic research, drug studies, and development biology [4]. Using the noninvasive UBM technique, a single animal can be monitored over an extended time period without being sacrificed for each imaging experiment.

1.4 Ultrasound Transducer

Ultrasound transducer usually uses piezoelectric crystals to both generate and receive ultrasound. When applied electric field, these crystals will produce a strain, which in turn generate ultrasound wave. Also, a mechanical displacement will create an electric potential, which makes the crystal an acoustic wave sensor. The piezoelectric crystals are the heart of the transducer as it converts the electrical energy to acoustic energy, and vice versa.

1.5 Transducer Arrays

Ultrasound arrays are essential in video rate imaging which requires rapidly steer and focus the receive aperture over the desired field of view. The geometry for a typical B-mode image formed by a one-dimensional (1-D) linear array is shown in Fig. 1.2a. A two-dimensional (2-D) array is necessary to form a “C-mode” image, where the image plane is parallel to the array (see Fig. 1.2b). Three dimensional imaging is possible by stacking multiple C-mode image planes (see Fig. 1.2c).

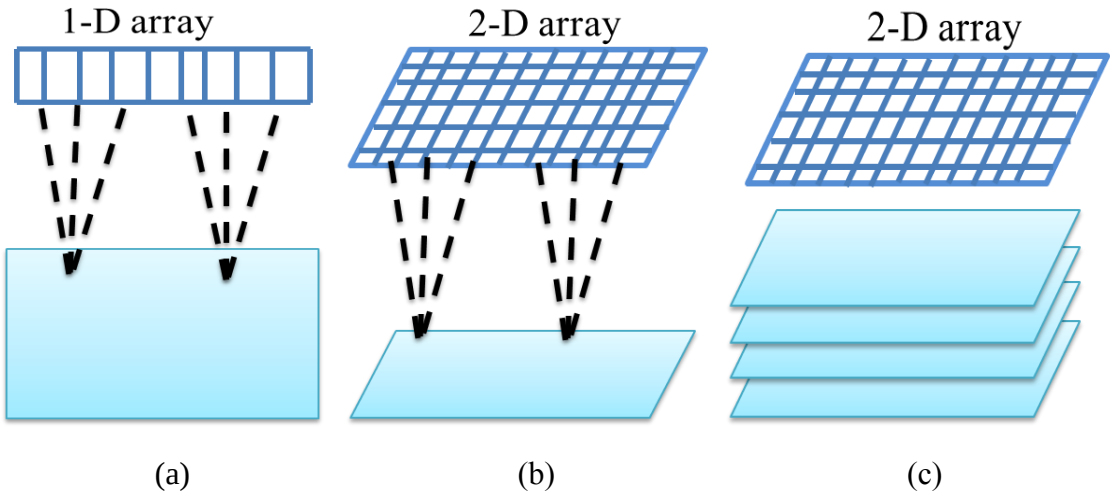

Figure 1.2 **(a) Geometry for typical B-mode image by 1-D array. (b) Geometry for typical C-mode image by 2-D array. (c) Possible 3-D imaging.**

1.6 High Frequency Arrays for UBM

For ultrasound array, in order to suppress aliasing in the reconstructed image, the size of array elements should be comparable to ultrasound wavelength. Also, the thickness of the piezoelectric crystal in transducer is determined by the desired frequency. In principle, a video rate UBM system requires a high frequency transducer array. Therefore, higher frequency arrays require smaller elements. In practice, high frequency arrays do not exist due to major fabrication and integration challenges. 1-D arrays higher than 35 MHz have proven to be extremely difficult to fabricate due to excessive challenges in dicing sufficiently small array elements and establishing electrical connections [5]. Lower frequency 2-D array scanners with roughly 60 × 60 elements have become available for real-time volumetric imaging [6]. However, the fabrication techniques for these "Matrix Transducers" are essentially the same as for 1-D arrays. Considering that high frequency 1-D arrays and data acquisition electronics are already challenging to fabricate. High frequency 2-D arrays for UBM represent a monumental challenge with major problems include dicing piezoelectric crystal to micro-scale elements, crosstalk between elements, electrical connections as well as lack of quality high frequency materials and electronics.

1.7 Optoacoustic Detection

Optical techniques are an attractive alternative for detecting high frequency ultrasound. This is sometimes referred to as "optoacoustic" detection [7]. Optical detection of ultrasound has been studied for several decades. The principle is straightforward: a laser beam probing an optically reflective surface exposed to the incident ultrasound wave, the displacement caused by ultrasound wave will modulate the reflected laser. As depicted in Fig. 1.3[8], the Fabry-Perot interferometer structure,

also known as an etalon, is one of the simplest and effective approaches for optoacoustic detection.

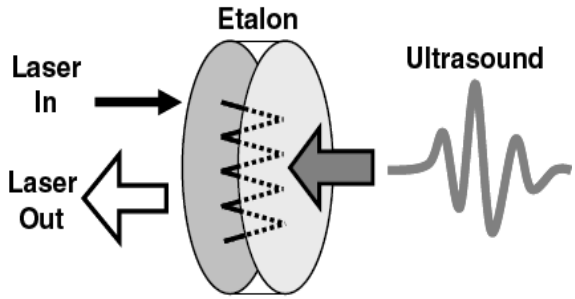

(a)

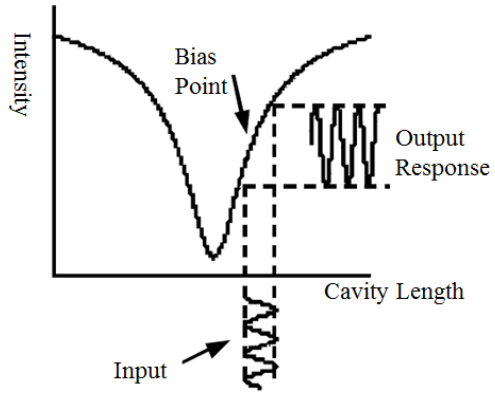

(b)

Figure 1.3 (a) Basic geometry for an etalon optoacoustic sensor. (b) Ultrasound modulates the etalon thickness, which in turn change the reflected laser intensity.

Etalon detection of ultrasound was first proposed by Thomson [9]. Beard [10] [11] build an etalon based hydrophone with detection sensitivity comparable to that of conventional piezoelectric hydrophones when operating at medical diagnostic frequency range.

Optoacoustic etalons have many advantages over conventional piezoelectric arrays. First, the active sensing area and the spacing of array elements are defined by the spot size of the optical beam, which can be easily reduced to few microns using conventional optics. Second, the optical signal modulated by ultrasound pulse is extracted using optical detector, thus no electronic connections are needed. Third, detection frequencies around the 100 MHz regime are well within the range of conventional optical detectors, which can exceed 1GHz. Also, bandwidth can be improved by reducing etalon bulk thickness or choosing appropriate material. Considering above factors, we can conclude that optoacoustic detection of ultrasound easily achieves spatial resolution and bandwidths for high frequency UBM arrays.

Our preliminary study shows that optical techniques provide high sensitivity, broadband ultrasound detection, large dynamic range and massive parallel readout capability, making it possible to explore a completely different approach to build UBM systems. In this paper, we build the ultrasound receiver and transmitter separately, and hope to combine ultrasound generation with etalon detection together since both transmits and receives ultrasound are essential for real-time ultrasound imaging.

Chapter 2

ETALON DETECTION

An etalon, which is a Fabry-Perot resonator, is the essential part for "optoacoustic" ultrasound detection. It serves as an optical interferometer, detecting ultrasound by converting changes in the cavity length to intensity variation of the laser beam.

2.1 Basic Structure of Etalon

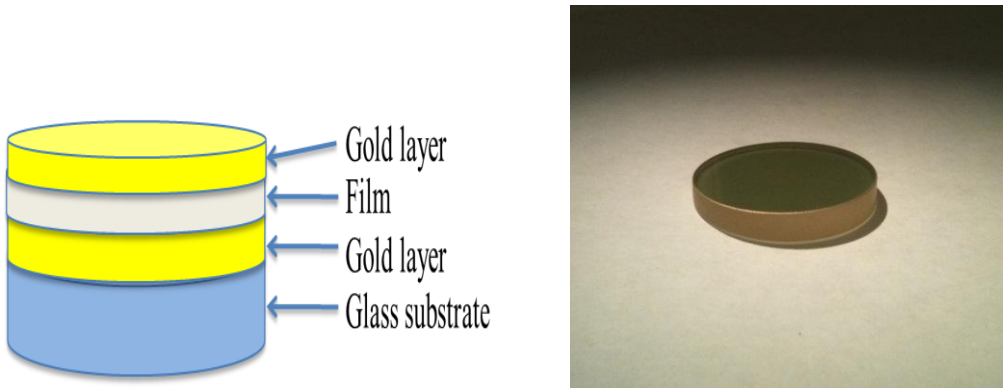

(a) (b)

Figure 2.1 (a) The structure of etalon (b) A picture of etalon

An etalon usually includes a glass substrate and three layers: one transparent film and two partially reflecting mirrors. The transparent film, serves as the optical cavity, is sandwiched between two partially reflecting mirrors. Gold is chosen as the material for the reflector due to its high reflection coefficient. SU-8 photoresist, polystyrene microsphere, parylene have been investigated separately as the transparent film. Fig. 2.1 shows the structure of an etalon.

2.2 Fabry-Perot Interference

Etalon, which is a Fabry-Perot resonator, is based on the Fabry-Perot interference. Here is a brief introduction of Fabry-Perot interference.

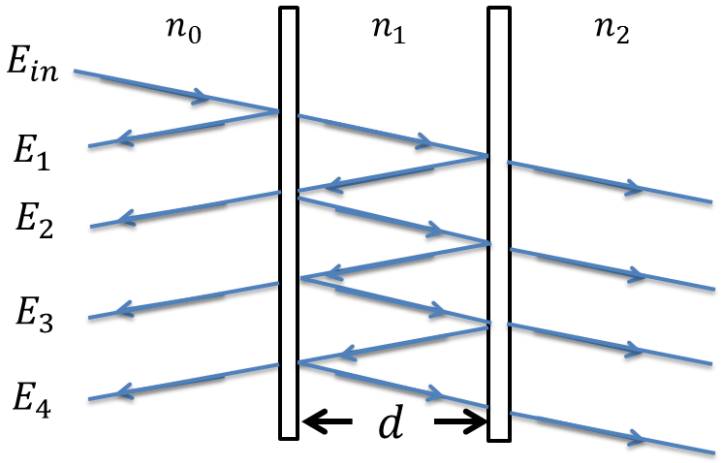

Figure 2.2 The light path within the etalon

As shown in Fig. 2.2, two patially tansmissive mirrors are at a distance d from each other and both have a reflection coefficient R . Suppose that the absorption within the mirror being ignored, the transmission coefficient should be (1- R). Light E_{in} incident from an external source undergoes multiple beam interference within these two mirror, producing a reflected and a transmitted signal. Suppose the incident angle is 90 degree, and the refractive index from left to right is: n_0, n_1, n_2 . $r_{01}$is the reflection coefficient when ligth propagate from medium 0 to medium 1. t_{01} is the transmission coefficient when ligth propagate from medium 0 to medium 1. The reflected signal is

$$\begin{aligned} E_r = r_{01}E_{in} &+ t_{01}r_{12}t_{10}E_{in}e^{-j\phi} \\ &+ t_{01}r_{12}t_{10}E_{in}e^{-j\phi}\left(r_{10}r_{12}e^{-j\phi}\right) \\ &+ t_{01}r_{12}t_{10}E_{in}e^{-j\phi}\left(r_{10}r_{12}e^{-j\phi}\right)^2 + \cdots \\ &+ t_{01}r_{12}t_{10}E_{in}e^{-j\phi}\left(r_{10}r_{12}e^{-j\phi}\right)^n \end{aligned}$$

n is a very large number here because the light will bounce back and forth for many times.

$$\begin{aligned} \frac{E_r}{E_{in}} &= r_{01} + t_{01}r_{12}t_{10}E_{in}e^{-j\phi}\frac{1-\left(r_{10}r_{12}e^{-j\phi}\right)^n}{1-\left(r_{10}r_{12}e^{-j\phi}\right)} \\ &= \frac{r_{01} + r_{12}e^{-j\phi}(t_{01}t_{10} - r_{01}r_{10})}{1-\left(r_{10}r_{12}e^{-j\phi}\right)} \end{aligned}$$

If n_0, n_1, n_2 are all real numbers. Then $t_{01}t_{10} - r_{01}r_{10} = 0$

So we get the reflection coefficient of the etalon, which is

$$R_{etalon} = \frac{r_{01} + r_{12}e^{-j\phi}}{1 - (r_{10}r_{12}e^{-j\phi})} \times \frac{r_{01} + r_{12}e^{+j\phi}}{1 - (r_{10}r_{12}e^{+j\phi})}$$

We assume that $r_{01} = -r_{10} = r, r_{12} = -r_{01}$, then

$$\begin{aligned} R_{etalon} &= \frac{r - re^{-j\phi}}{1 - (r^2e^{-j\phi})} \times \frac{r - re^{+j\phi}}{1 - (r^2e^{+j\phi})} \\ &= r^2 \times \frac{2(1 - cos\phi)}{1 - 2r^2cos\phi + r^4} \\ &= \frac{4r^2}{(1 - r^2)^2} \times \frac{\sin(\phi/2)^2}{1 + \frac{4r^2}{(1 - r^2)^2}\sin(\phi/2)^2} \end{aligned}$$

Assume $R = r^2$, then

$$R_{etalon} = K \cdot \frac{\sin(\phi/2)^2}{1 + K\sin(\phi/2)^2}$$

Therefore, we get $I_R = I_0 R_{etalon}$

$$I_R = I_0(1 - \frac{1}{1 + Ksin^2(\phi/2)})$$

Where the phase is $\phi = \frac{4\pi n_1 d}{\lambda} = \frac{4\pi n_1 d\upsilon}{c}$, $K = \frac{4R}{(1-R)^2}$ here n_1 is the refractive index of the medium within two mirrors, λ is the laser wavelength.

Fig. 2.3 shows the typical reflection coefficient spectrum for Fabry-Perot interference with different R.

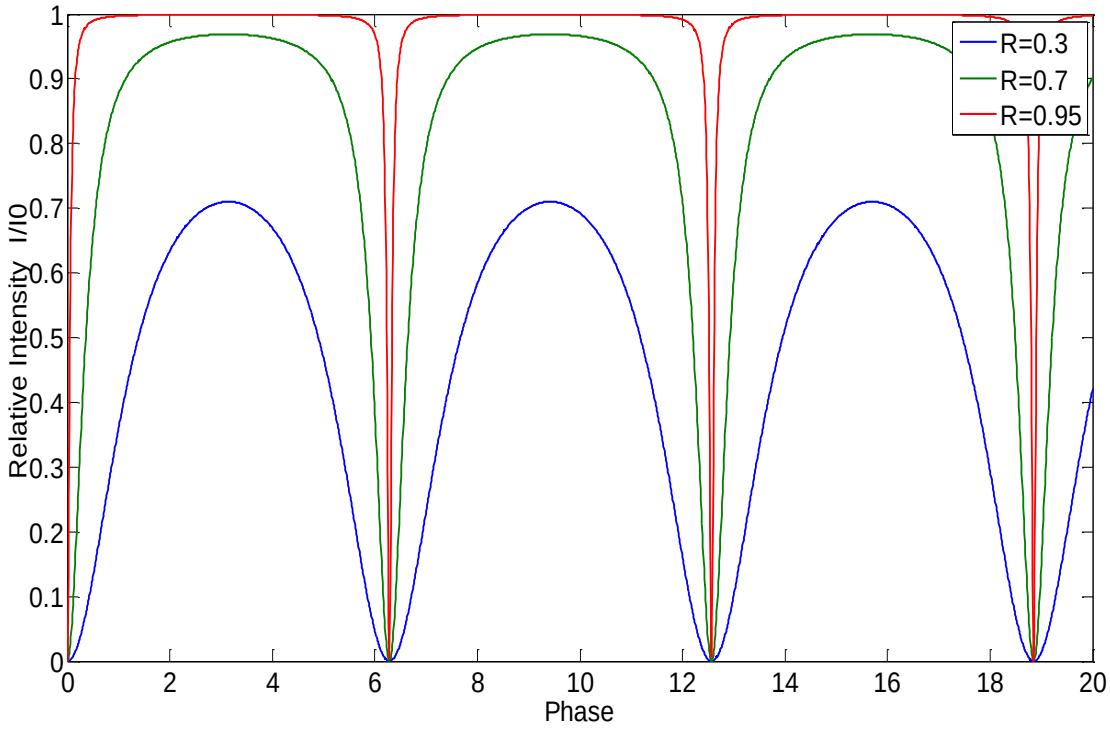

Figure 2.3 The reflection coefficent in a Fabry Perot interference with different R

The position of the resonace dip should be at $\phi = 2m\pi$, where m=1,2,3,… Each m here represents a resonance mode. Also, we will notice that the larger the R, the sharper the slope near resonance dip.

The distance between two resonance dip is known as the Free Spectral Range (FSR), which is usually given in Hz. It represents how much the light

frequency have to change for the Febry-Perot resonator to move from one resonace mode to the next. The expression for FSR is:

$$\text{FSR} = \frac{C}{2nd}$$

The width of the resonance at full width half maximum, $\Delta\upsilon$ is

$$\Delta\upsilon = \frac{C}{\pi nd\sqrt{K}}$$

The finesse, essentially the Q of the resonator, is the ratio of the free spectral range to the bandwidth of resonance dip.

$$\text{F} = \frac{FSR}{\Delta\upsilon} = \frac{\pi\sqrt{K}}{2}$$

Finesse serves as an amplication term for the optical path length in etalon. Under the same condition, larger finesse will produce larger optical signal in optoacoutic imaging.

2.3 The Thickness of the Gold Layer

From Fig. 2.3 we can see that the width of the resonance will become smaller as the reflection coefficient goes larger. And we know that the sharper the slope, the better sensitivity the etalon. Intuitively we want to increase the thickness of the gold layer to increase the reflection coefficient. But, here we must consider the optical loss in the gold layer since gold is not a dielectric material. Previous analysis

ignore the fact that there is absorption in the gold layer. However, once the gold layer is too thick that large loss is induced, then strong interference will not be expected. Choosing the proper thickness is a matter of trade-off between reflectioin coefficient and optical loss.

First, we need to notice that gold has a complex refractive index

$$n = n' + ik$$

The real part of the refractive index n represents the phase speed, while the imaginary part k indicates the amount of absorption loss when the electromagnetic wave propagates through the material. k is often called the extinction coefficient. Both n' and k are dependent on frequency. In order to find the optimal gold layer thickness, we first need to investigate the relation between n', k and frequency. From [12] we will find a chart describing this relation. Fig. 2.4 shows these values and an approximate fitting curve.

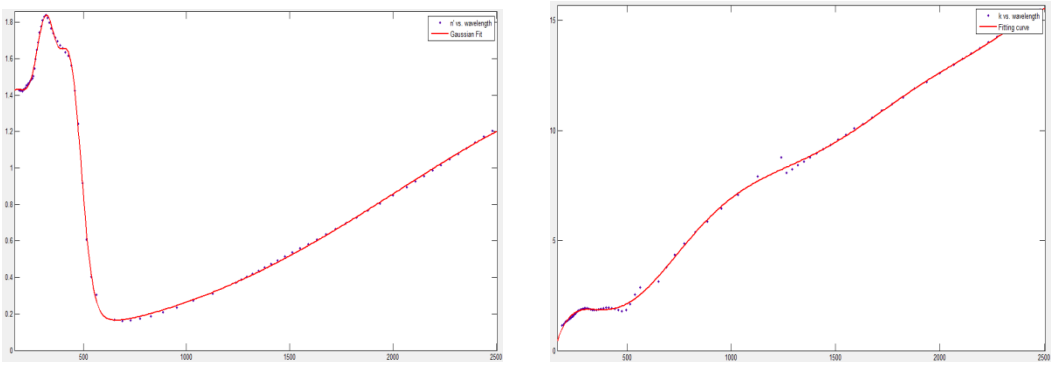

(a) (b)

Figure 2.4 (a) The real part of refractive index of gold and its fitting curve. (b) The imaginary part of refractive index of gold and its fitting curve.

The expressions for the fitting curves of n' are:

$$n'(x) = \sum_{i=1}^{4} ai \times e^{-((x-bi)/ci)^2}$$

a1	b1	c1	a2	b2	c2	a3	b3	c3	a4	b4	c4
0.7	323.1	65.1	1.44	3246	1722	1.12	437.9	76.6	1.36	170.7	226

The fitting curve for k is:

$$k = \sum_{i=0}^{9} Pi \times x^i$$

P0	P1	P2	P3	P4
-14.12	0.1788	-7.899×10^-4	1.779×10^-6	-2.248×10^-9
P5	P6	P7	P8	P10
1.702×10^-12	-7.875×10^-16	2.173×10^-19	-3.268×10^-23	2.045×10^-27

So now we can use these expressions to approximate the n' and k value at any given wavelength.

However, before we take further steps, we need to take a closer look at the etalon.

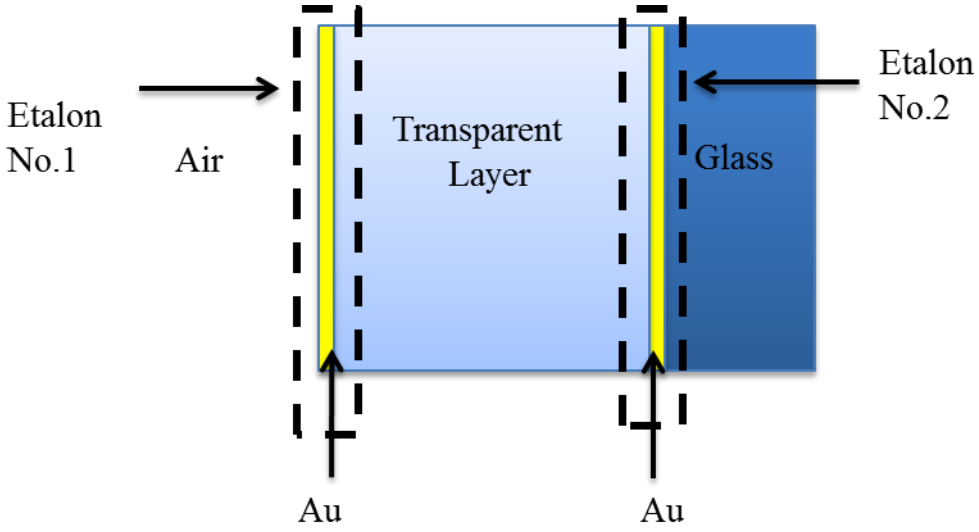

Figure 2.5 More detailed etalon structure.

Fig. 2.5 shows a more realistic picture of etalon in which the thickness of gold layer is taken into account. In this picture we notice that in order to have a thorough analysis of etalon, we need to break the etalon into three smaller ones: Etalon No.1 formed by air, gold layer and the transparent layer, which is indicated by the first dash-line rectangle; Etalon No.2 formed by transparent layer, gold layer and glass substrate, which is indicated by the second dash-line rectangle; and the original etalon formed by air, transparent layer and glass substrate. In etalon No.1 and No.2, laser beam will bounce back and forth within the gold layer, cause large loss.

Previously we have

$$\frac{E_r}{E_{in}} = r_{01} + t_{01}r_{12}t_{10}E_{in}e^{-j\phi}\frac{1-\left(r_{10}r_{12}e^{-j\phi}\right)^n}{1-(r_{10}r_{12}e^{-j\phi})}$$
$$= \frac{r_{01} + r_{12}e^{-j\phi}(t_{01}t_{10} - r_{01}r_{10})}{1-(r_{10}r_{12}e^{-j\phi})}$$

And we made assumptions that n_0, n_1, n_2 are all real numbers and $r_{01} = -r_{10} = r, r_{12} = -r_{01}$. Now these assumptions can't be justified anymore. Our strategy is straightforward: First we get the reflection and transmission coefficient for Etalon No.1; then we get the same information from Etalon No.2. In the end, instead of using a fixed real number as the reflection index of the two mirrors, we use these more accurate complex numbers.

Fig. 2.6 shows the simulated reflection coefficient of etalon and the first order derivative of reflection coefficient. Laser beam is incident on the glass substrate side. Parylene with a thickness of 6800 nm is chosen as the transparent layer. Gold layer thickness is chosen to be 30 nm, 45 nm, 80 nm.

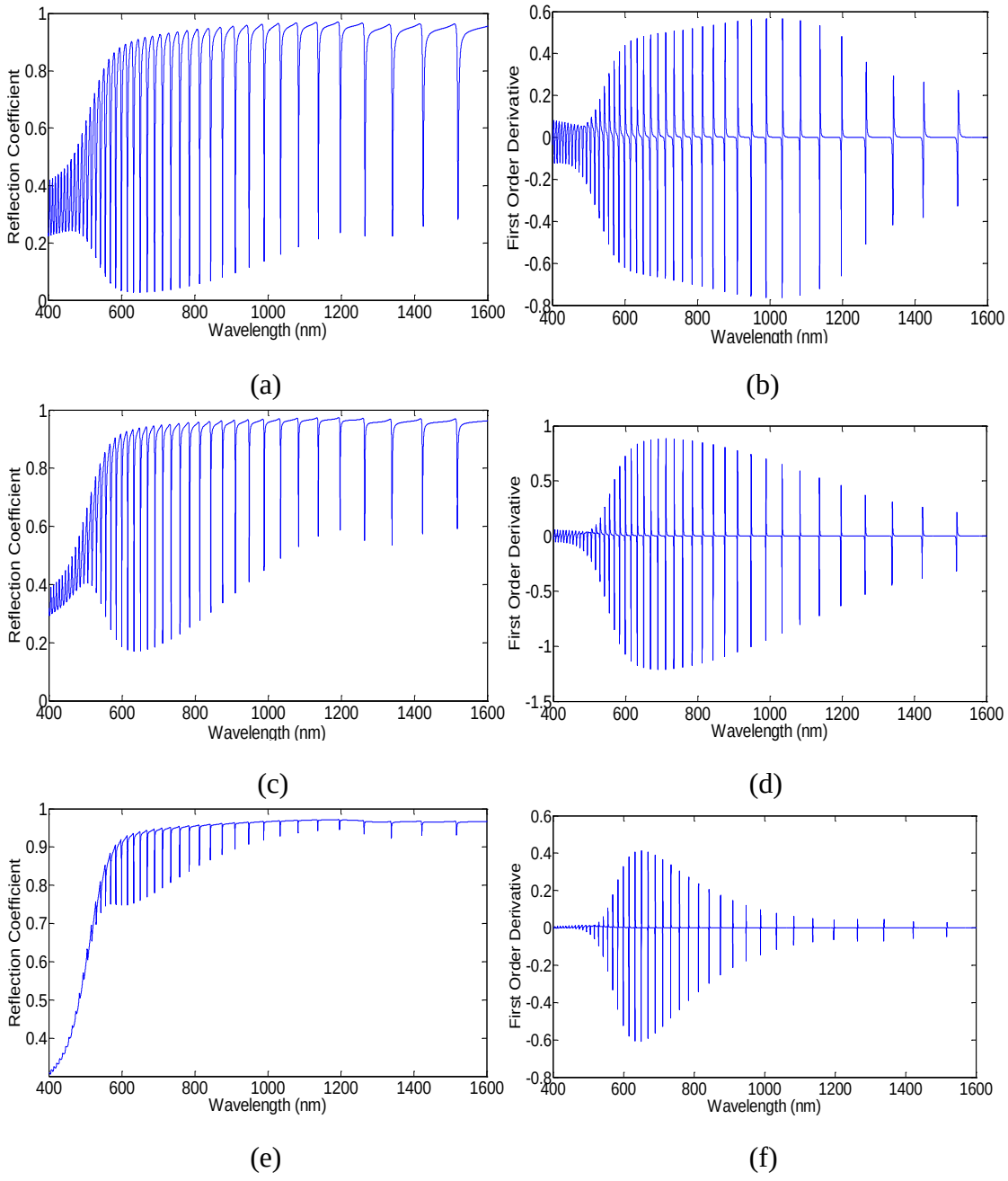

Figure 2.6 **(a)(c)(d) are the simulated reflection coefficient of etalon with gold layer of 30, 45, 80 nm respectively. (b)(d)(f) are the simulated first order derivative of reflection coefficient of etalon with gold layer of 30, 45, 80 nm respectively.**

To demonstrate the theory, we made two etalon using SU-8 2005 photoresist. The thickness of the etalon is 585 nm, which is the reason that the FSR is larger than the simulated one. Two different thickness of gold layer is chosen here, one is 45 nm and one is 80 nm. Fig. 2.7 shows the spectrum of these two etalons.

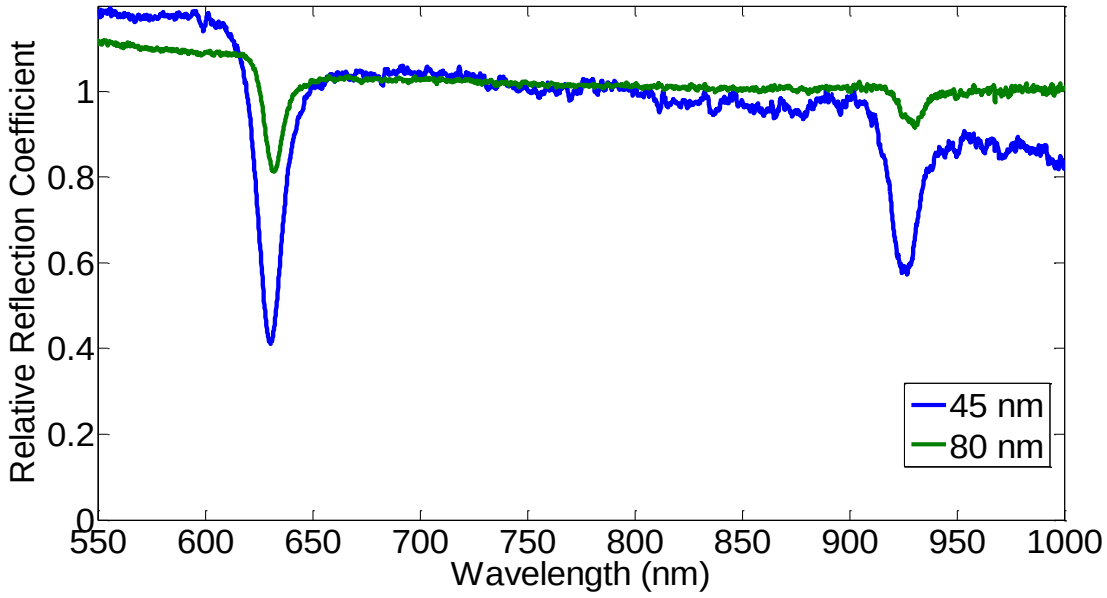

Figure 2.7 Spectrum of etalons with 45 nm and 80 nm thickness gold layer

From the figure we can see that the etalon with 45 nm gold layer has a sharper resonance slope than the one with 80 nm gold. This observation matches our theory.

In order to find out the optimal gold layer thickness, we have to investigate the simulated data. We notice that from 30 nm to 45 nm, the maximum value of first order derivative of reflection coefficient goes larger because of the higher reflection coefficient of thicker gold layer. However, comparing 45 nm and 80 nm, we can clearly see that the maximum number goes smaller because of the loss within the thick gold layer. Fig. 2.8 shows this Gaussian shape trend.

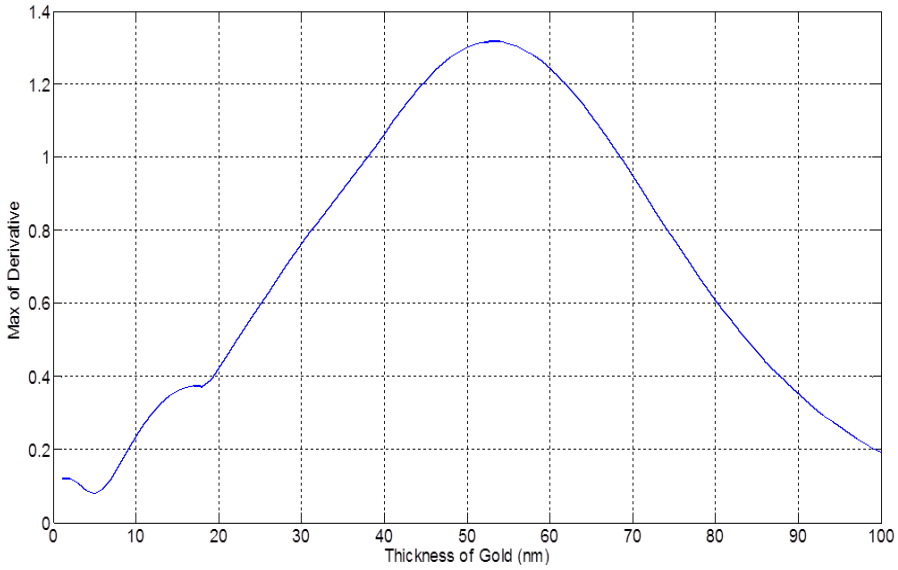

Figure 2.8 The maximum value of derivative of reflection coefficient with different thickness of gold

We will notice that 53 nm thickness gold layer will produce the maximum derivative of reflection coefficient. However, 53 nm is not our best option because we use a 785 nm AlGaAs diode laser in our experiment, and this maximum value doesn't fall right around 785 nm. From Fig. 2.6(d), we can see that the maximum value, which is around -1.2, falls right into the 785 nm area. Therefore, a gold layer thickness of 45 nm is chosen in our experiment.

2.4 The Transparent Layer in Etalon

After choosing the thickness of gold layer, we then need to focus on the transparent layer. Because we use etalon as an ultrasound array for parallel detection, the sensitivity of the each element should be the same, which requires that the transparent layer to be uniform. Therefore, uniformity is our priority when choosing proper transparent layer. Also, this layer should be relatively soft. In our experiment, we investigate three different materials: polystyrene microspheres, SU-8 photoresist and parylene.

Polystyrene microspheres are widely used in cell biology studies, and are available in various sizes from 10 nm up to tens of microns. They can be made into well-ordered two-dimensional arrays by self-assembly [13], a commonly used technique in nanotechnology. For many years, self-assembled arrays have been investigated for photonic crystals [14] and chemical sensors [15]. The ability to produce a sub-micron thick monolayer in a consistent manner suggests its potential for realizing extremely thin optoacoustic sensors.

SU-8 photoresist is a high contrast; epoxy based negative photoresist designed for micromachining and other microelectronic applications. Using spin-coating method, it can be spread over a thickness ranging from few hundred

nanometers to hundreds of microns. Because it is a photoresist, it can be exposed and subsequently thermally cross-linked by exposing to UV light, leaving a thin, uniform layer [16].

Parylene is the generic name for a variety of polymers used as protection coating for electronics, aerospace and medical applications. Its special features include low dielectric constant, optical clarity and surface conformability. The reason we choose parylene as an option is because parylene can be deposited using chemical vapor deposition process, which has more precise thickness and uniformity control over other method.

2.5 Fabrication of Etalon

Fabrication of etalon begins with glass substrate. We use a 1 inch diameter round glass window (Edmund Optics) as substrate. Then, a 45 nm gold layer is coated on top of glass substrate using an evaporator. The gold layer serves as partially reflective mirror. Usually a layer of titanium will be coated between gold layer and glass as an adhesion promoter. However, we observe severe oxidation of this titanium layer. One possible explanation would be that the thickness of gold layer is too thin to stop the air in contact with titanium layer. In the end we coat gold layer without the titanium layer. Depending on the material, we will coat the transparent layer using different method. We will discuss this in detail later. After the transparent layer is finished, another 45 nm gold layer is deposited on the top of the transparent layer. As a final step, an additional 3 μm thick polydimethylsiloxane (PDMS) layer is spin-cast over the entire etalon surface for protection. The PDMS is diluted with heptane in a 1:1 ratio to make sure it can be spun to a thin layer. A sketch of the side view of etalon and a photo is shown in Fig. 2.1.

For the different transparent layer material, we have different methods to coat them.

2.5.1 Polystyrene Microsphere

Because polystyrene microsphere can float on water surface, we use dip-coating to coat the layer. An aqueous solution of 0.35 um diameter polystyrene microspheres (2.5%) was diluted with ethanol in a 1:1 ratio. Then we distribute approximately 100 uL this mixture over a microscope glass slide. This slide is slowly immersed into the surface of the water in a 100 mL container. As shown in Fig. 2.9(a), the microspheres distribute themselves on the water surface to form several regions of floating monolayers. Close-packed monolayers show strong optical diffraction, while amorphous monolayers only produce optical interference. The arrays are consolidated by adding 10 uL of a surfactant (1% sodium dodecylsulfate) to water surface [17]. As shown in Fig. 2.9(b), a glass slide is placed under the floating monolayers. When the glass slide is slowly lifted, both close-packed monolayer regions and amorphous regions will be left on the glass substrate [18]. Fig. 2.9 (c) shows the etalon defined by microsphere and gold layer. A scanning electron microscopy (SEM) image is shown in Fig. 2.9 (d).

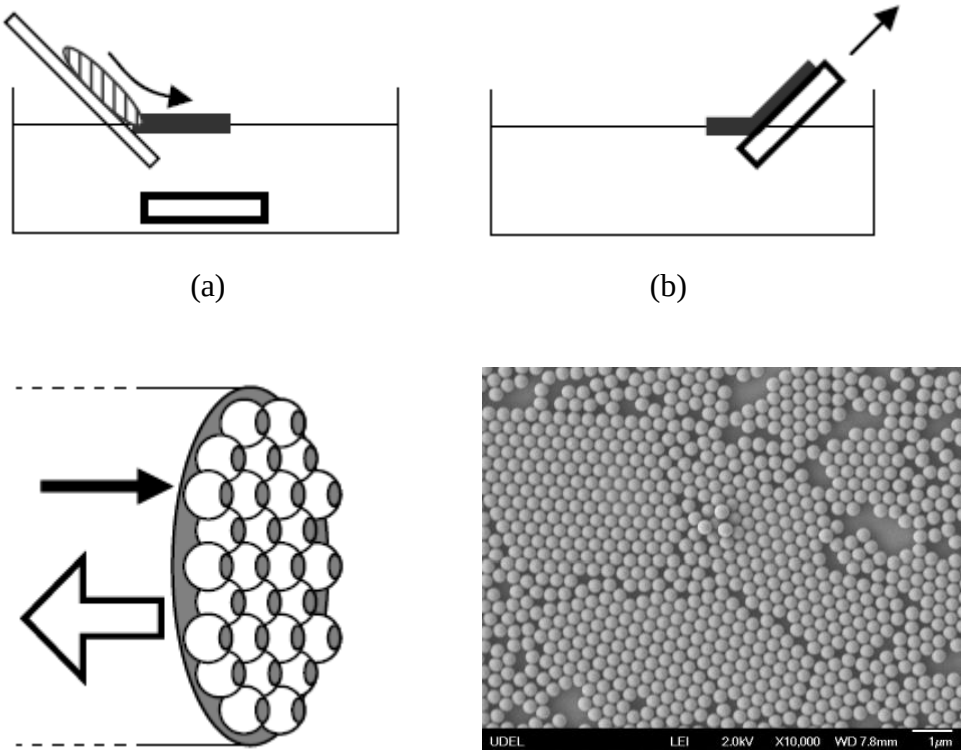

Figure 2.9 **(a) Using a glass slide to distribute the polystyrene microspheres on the surface of water. Another glass slide is placed underneath the monolayer. (b) Transfer the microsphere monolayer onto the glass slide. (c) Etalon defined by a gold layer deposited on the microspheres and substrate. (d) SEM image showing both close-packed and amorphous monolayer arrays.**

2.5.2 SU-8 2005 photoresist

SU-8 2005 photoresist is a typical photoresist; we use spin-coating method to coat the layer.

a. Substrate Preparation. Before the spin-coating process, the substrate should be cleaned and dried to achieve maximum process reliability. Acetone, methanol and isopropyl are used sequentially to clean the substrate, followed by a de-ionized water rinse.

b. Coating. A transparent layer of 6800 nm thickness will provide us a resonance dip near 785 nm. For spin coating method, the thickness of the layer depends on the rotation speed of the spinner. So after several attempts, we get the recipe to achieve this thickness. First, we dispense the resists to cover the entire surface. Then, we place the sample on the chuck of a spinner (Headway PWM32), spin at 500 rpm for 6 seconds with acceleration of 100 rpm/second. In the end, spin the sample at 1500 rpm for 30 seconds with acceleration of 300 rpm/second.

c. Soft Bake. Soft bake is performed to drive the solvent out of the photoresist. A level hotplate with good thermal control and uniformity is used. Soft bake time depends on the thickness of the layer. In our case, the 6800 nm layer will require 95 degree baking for 2-3 minutes.

d. Exposure. Exposure is used to cross-link the molecules in the photoresist; it is the most important step in spin coating. A UV light of peak wavelength near 350 nm is need. In our experiment, we use a mask aligner (Karl Suss MJB3) for exposure. For a thickness 6800 nm, the required exposure energy is 110-140 mJ/cm^2.

e. Post Exposure Bake (PEB). PEB is performed to promote the cross-link in the exposed area. So it should take place directly after exposure. The sample

will be placed on the hot plate of 95 degree for 3-4 minutes.

f. Hard Bake (cure). In the etalon sample, the photoresist layer serves as part of the final device. Therefore, though SU-8 2005 has good mechanical properties, a hard bake or final cure should be added to ensure that SU-8 2005 properties do not change in actual use. We use hot plate to bake the sample at 150 degree for 10 minutes. Also, the hard bake step is useful for annealing any surface cracks.

In the end, we found that SU-8 photoresist will slowly absorb water, making the layer expand. Thickness control is crucial in our experiment, so water absorption must be avoided. In our case, we use silicon to seal the rim of the sandwiched gold-photoresist-gold stack.

2.5.3 Parylene

Due to device limitations, we sent our samples to Material Research Institute in Penn State University to help us coat the parylene layer. Among the various parylene material, parylene C is chosen because it is the most widely used parylene. Thickness control is easier for parylene C. Like the photoresist sample, the parylene layer thickness is also 6800 nm.

Generally, the coating cycle begins with heating the raw parylene material (dimer) at 150 degree to vaporize it. The dimeric gas will be split to monomer by increasing the temperature to 650 degree. The monomer gas then flow to a vacuumed chamber where the sample is placed. In the end the gas will disperse and polymerize on the sample surface at room temperature to form parylene film.

2.6 Optical Characterization of Etalon

Before we use etalon for ultrasound detection, the optical resonance of the etalon must be characterized to evaluate its performance and determine the laser wavelength. Fig. 2.10 shows the basic experimental setup for optical characterization.

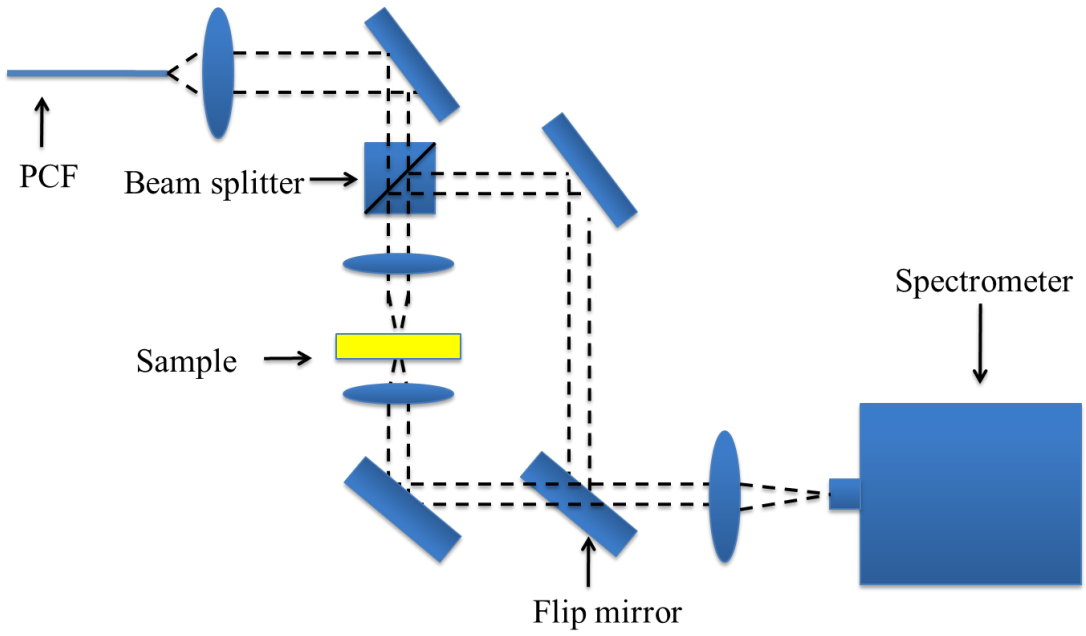

Figure 2.10 Block diagram of the experimental setup for optical characterization

A Q-switched Nd:YAG microchip laser (NP10820-100, Teem Photonics)

is used as laser source. It producers 0.6 ns duration pulses at 1064 nm with 8 μJ of energy at a 6.6 KHz repetition rate. A lens couples the pulse into a 7 m long photonic crystal fiber (PCF) with zero dispersion wavelength at 1040 nm (Crystal Fibre, Inc.). The photonic crystal fiber (PCF) dramatically enhances the nonlinear optical propagation. Therefore, a white color beam with relatively flat spectrum will come out of the fiber, making it a perfect light source for optical characterization.

The Laser beam then travel through a beam splitter and is focused onto a spot on the surface of the etalon. The reflected light will travel through the beam splitter again and then is focused into a spectrometer (Thorlab Inc., SP2-USB spectrometer) connected to the computer for data acquisition. The transmitted light will also be focus into the same spectrometer.

Fig. 2.11 shows the optical spectrum of SU-8 photoresist etalon and parylene etalon. For SU-8 etalon, the FSR is 8 45125 ×10^12 Hz, the optical bandwidth is 1 405241 ×10^12 Hz, and finesse is 6.01. For parylene etalon, the FSR is 6 333302 ×10^12 Hz, the optical bandwidth is 0 673549 ×10^12 Hz, and finesse is 9.40. The criteria of a good etalon are its uniformity and finesse. SU-8 etalon is build using spin-coat method, while parylene etalon is built using evaporation. Evaporation has a better thickness control over spin-coat method, thus the parylene etalon obtains better uniformity than SU-8 etalon. And our observation demonstrates this phenomenon. Therefore, parylene etalon is more suitable for parallel detection.

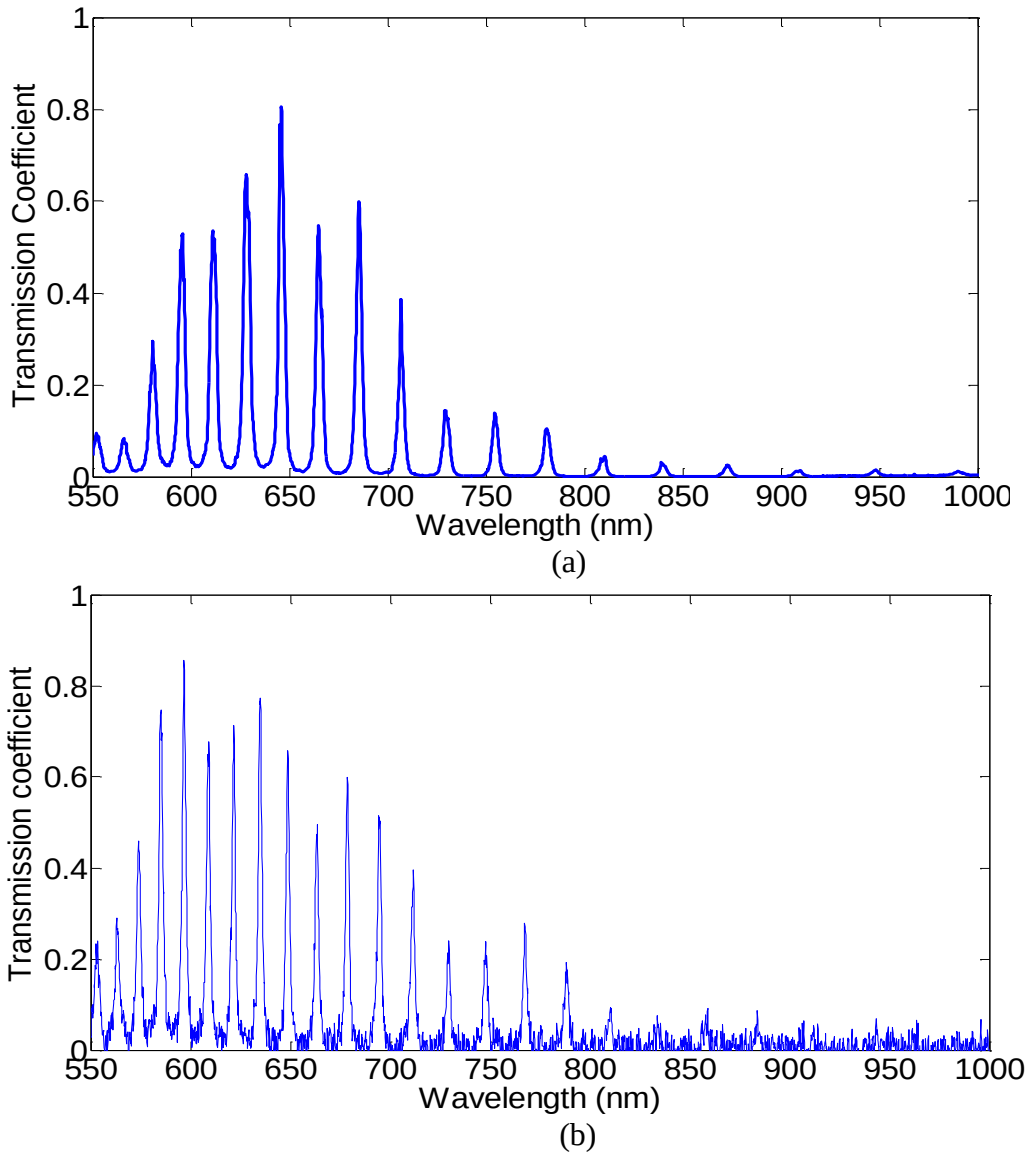

Figure 2.11 (a) Optical spectrum of SU-8 etalon. Gold layer thickness is 45 nm; SU-8 layer thickness is 6800 nm (b) Optical spectrum of parylene etalon. Gold layer thickness is 45 nm; parylene layer thickness is 8100 nm.

2.7 Ultrasound Characterization of Etalon

After we choose the etalon that is suitable for optoacoustic detection, we can start to characterize its ultrasound property.

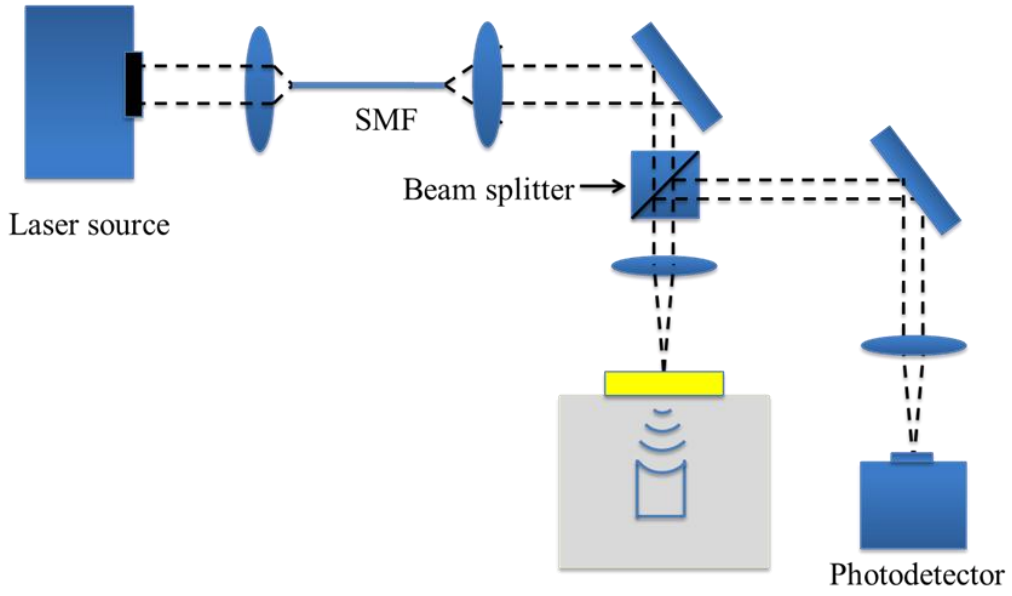

Figure 2.12 Block diagram of the experimental setup for ultrasound characterization

As shown in Fig. 2.12, a 785 nm AlGaAs continuous-wave (CW) diode laser is used in our experiment as the laser source. A lens couples the beam into a single mode optical fiber. Another lens is used to collimate the beam coming out of the

fiber. Then the beam travels through a beam splitter and is focused onto the surface of the etalon mounted at the wall of a water tank. The reflected light travels through the beam splitter again and is focused into an amplified InGaAs photodetector connected to the computer for data acquisition.

Fig. 2.13 shows the ultrasound signal from SU-8 and parylene etalon. SU-8 etalon includes a 6800 nm thick SU-8 2005 layer and two 45 nm gold layer. The parylene etalon consists of one 8100 nm parylene layer and two 30 nm gold layer.

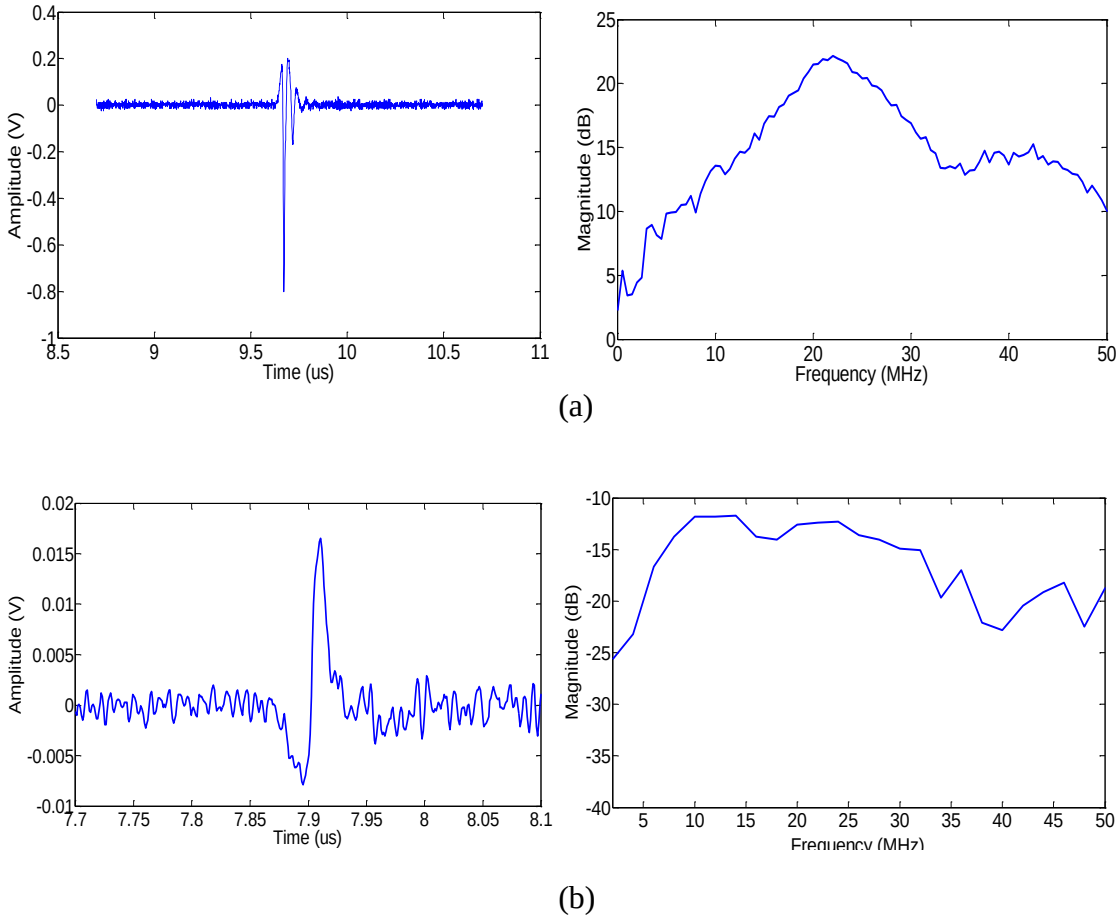

Figure 2.13 (a) Ultrasound signal from SU-8 2005 etalon and its spectrum. (b) Ultrasound signal from parylene etalon and its spectrum

From this figure we can see that under the same condition, the -6 dB bandwidth for SU-8 etalon and parylene etalon are 15 MHz and 28 MHz respectively. Again, the parylene etalon is chosen for its wider bandwidth.

2.8 Etalon Array

We built etalon array based on following hypothesis: small etalon has more space to deform than single piece etalon, thus obtains higher sensitivity and produces larger signal. This hypothesis is shown in Fig. 2.14.

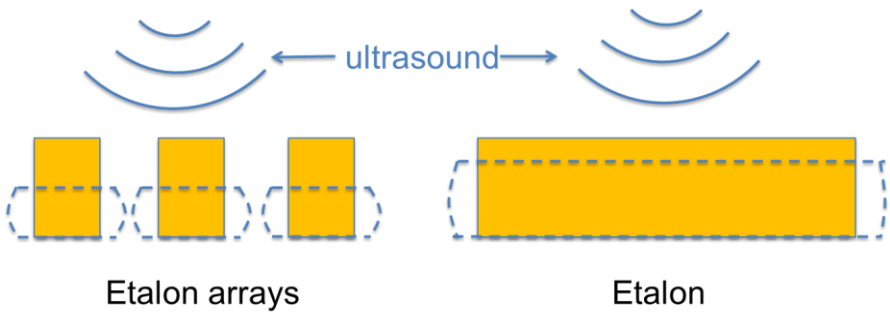

Figure 2.14 Etalon formed by smaller arrays tends to have larger deformation due to larger space.

SU-8 2005 is ideal to make etalon array because photoresist is used to produce patterns. A mask is designed using AutoCAD to produce the pattern of the

array. The mask is made of chrome with round holes on it. Each round area is 10 μm diameter, and the spacing between the round holes is 20 μm. The fabrication process is the same as described in 2.5.2, except that the mask is used in exposure step and SU-8 2005 layer is developed using SU-8 developer. Fig. 2.15 shows the AutoCAD design of the mask and the picture of etalon array.

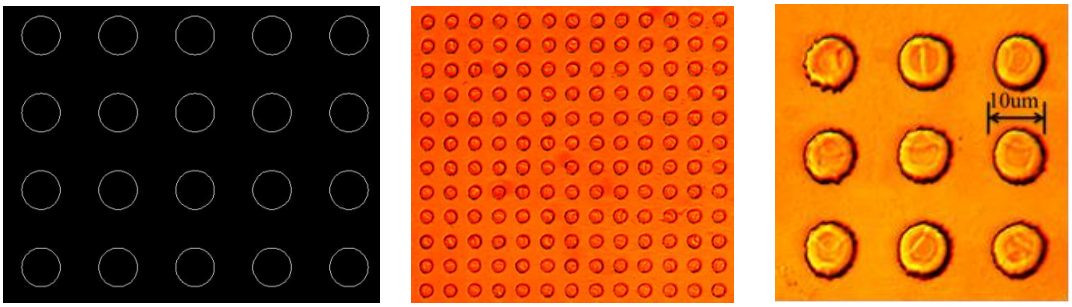

(a) (b) (c)

Figure 2.15 (a) AutoCAD design of the mask. (b) Picture of etalon array. (c) "zoom in" picture of etalon array

The optical and ultrasound characterization of etalon array follows the same procedure shown in 2.6 and 2.7. The focal spot on the etalon array is only around 6 μm diameter, so the laser beam have to be carefully aligned with the array element to make sure the laser will be focused in the center of array element. Figure

2.16 shows the result of optical spectrum of etalon array. This etalon array has a 6500 nm thick etalon layer and two 45 nm thick gold layer.

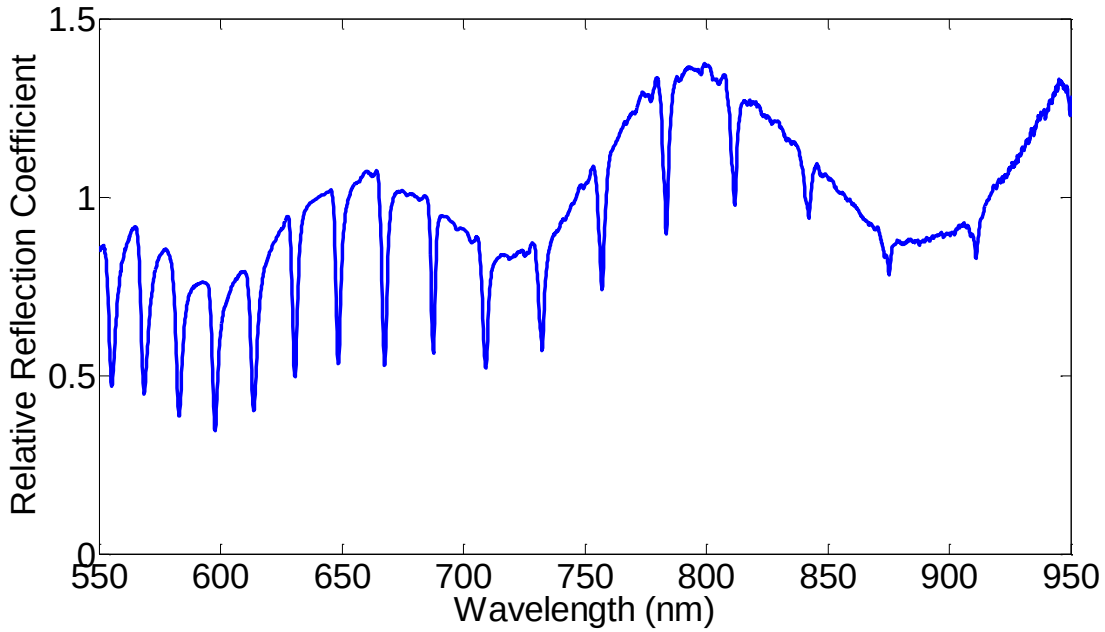

Figure 2.16 Optical spectrum of etalon array

From the figure we get that the FSR of etalon array is $8.473 \times 10^{12}\ MHz$, the optical bandwidth is $0.654 \times 10^{12}\ MHz$, the finesse is 12.96.

Fig. 2.17 shows the ultrasound signal from the etalon array.

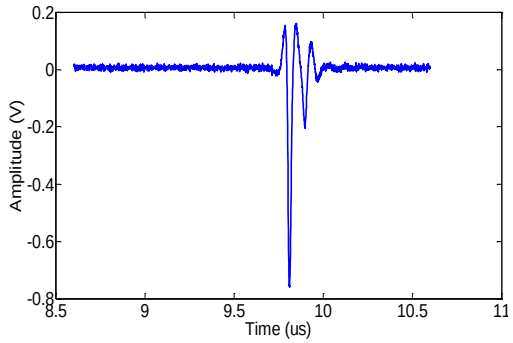

Figure 2.17 Ultrasound signal from etalon array

Comparing the Fig. 2.17 and Fig. 2.13 (a), we can see that the under the same condition, the peak to peak value of ultrasound signal is almost the same. There is no obvious improvement from etalon array.

Chapter 3

LITHIUM NIOBATE ULTRASOUND TRANSDUCER

Our final goal is to develop an ultrasound transducer that combined ultrasound generation with etalon detection. This is significant because a device that both transmits and receives ultrasound is essential for real-time ultrasound imaging. The most popular material for generating ultrasound is a polycrystalline ferroelectric ceramic material, lead zirconate titanate (PZT), which has very strong piezoelectric properties after being polarized. However, considering the etalon detection part, a transparent piezoelectric material should be used for ultrasound generation, while at the same time light will go through it. Obviously the opaque PZT will not be suitable in our application. Piezoelectric polymers such as polyvinylidene fluoride (PVDF) are a mature ultrasound transducer technology. Moreover, etalon sensitivity is maximized when the etalon cavity is a soft material, such as a polymer. However, our experiment found that the PVDF layer is not perfectly transparent, and the surface is not flat enough. It will not meet the demand for a uniform etalon. So we decide to use lithium niobate as the ultrasound transmitter, and find a way to combined it with our etalon.

3.1 Lithium Niobate

Lithium niobate is a transparent solid material; it is a compound of niobium, lithium and oxygen. Due to its crystal structure, lithium niobate is a ferroelectric material suitable for many applications. It shows ferroelectricity, piezoelectric effect and nonlinear optical polarizability. It is also transparent for

wavelengths between 350 to 5200 nm. Here we will use its piezoelectric property to build an ultrasound transducer. Table 3.1 shows relevant material properties of 36 degree rotated Y-Cut lithium niobate [Reported by Boston Piezo-optics, Bellingham, MA].

Table 3.1 The Properties of 36 degree Rotated Y-cut Lithium Niobate Wafer

Property	Value
Relative clamped dielectric constant ($\varepsilon^s/\varepsilon_0$)	39 [19]
Electromechanical coupling coefficient (k_t)	0.49
Mechanical quality factor (Q_m)	10000
Electrical quality factor (Q_E)	1000
Density (g/cm^3)	4.64
Longitudinal wave velocity (m/s)	7340
Acoustic impedance ($MRayl$)	34.0
Curie temperature (℃)	1150

Here the electromechanical coupling coefficient (k_t) is used to describe the ability of a material to convert one form of energy to another. The coefficient is

defined as stored mechanical energy/total stored energy. The total stored energy includes both mechanical and electrical energy [20]. From this table we can find that lithium niobate displays high longitudinal wave speed, low dielectric constant and high electromechanical coupling. All these factors make lithium niobate the ideal material for sensitive large aperture single element ultrasound transducer.

3.2 Piezoelectric Effect

We have briefly introduced the piezoelectric effect, where a mechanical stress will produce electrical field. Next we will have a closer look at this effect.

Piezoelectric effect can only be shown in crystals that have no center of symmetry. As we know, crystals are made of individual molecules, which have a polarization. One end of molecule shows positive charge while at the other end shows the negative charge. This pair is called a dipole. For a specific sample, the dipole density or polarization can be obtained by adding all the dipole moments together. Dipoles near each other tend to be aligned in regions. However, these regions are usually oriented randomly as shown in Fig. 3.1(a). In order to produce the piezoelectric effect, the crystal usually is applied a very strong electrical field at an elevated temperature, which is called the Curie temperature. This elevated temperature will allow the molecules to move freely and the strong electrical field will reorient all the dipoles in nearly the same direction. After the temperature is cooling down while the electrical field still present, the direction of the dipole will be stable in the reoriented direction. This process is shown in Fig. 3.1(b).

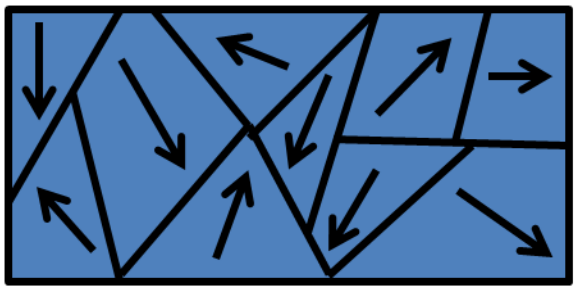

(a)

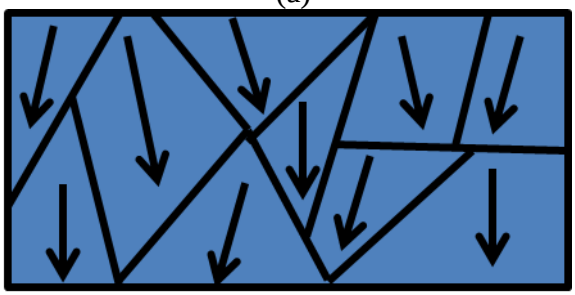

(b)

Figure 3.1 (a) Dipole regions are randomly oriented, no piezoelectric effect is show. (b) After placing the sample in strong electrical field at high temperature, the dipole region is reoriented at nearly the same direction.

The piezoelectric effect can now be observed in the crystal. When the crystal is compressed or expanded, the dipoles will be displaced, causing the electric polarization of the crystal. Conversely, if an external electric field is applied to the crystal, the crystal will also compress or expand. If an AC signal is applied then the crystal will compress and expand at the same frequency as the signal. And we simply

use this expansion or compression to generate ultrasound. In terms of energy, this process is an electrical-mechanical energy conversion.

3.3 Structrue of Lithium Niobate Ultrasound Transducer

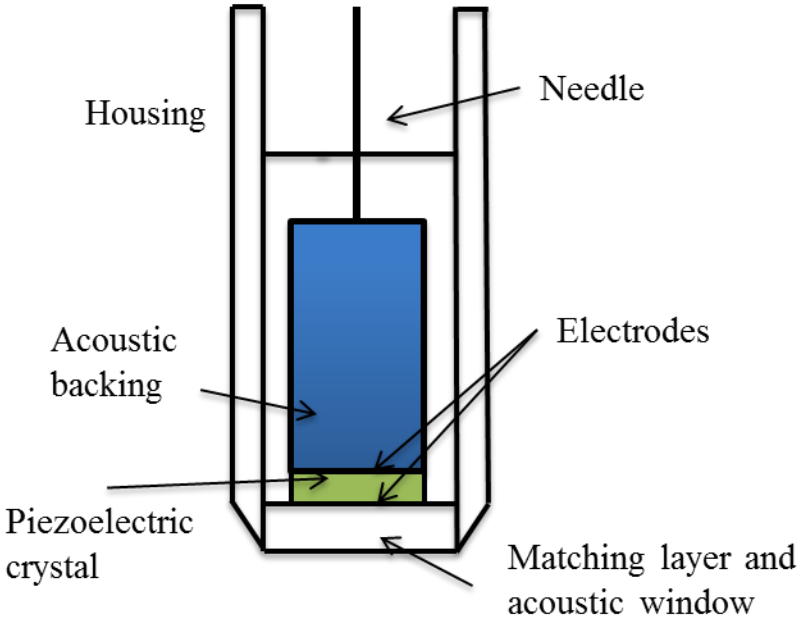

Figure 3.2 Structure of lithium niobate transducer

Fig. 3.2 shows the structure of the lithium niobate transducer [21]. The core part of the transducer is its acoustic stack includeing the piezoelectric crystal, matching layer and backing layer. The acoustic backing layer and the matching layer

are both electrical conductive. Each layer has different usage which we will illustrate later. The whole acoustic stack is mounted on a subminiature version A (SMA) male connector. Gold electrodes are coated on both faces of piezoelectric crystal. The front electrode will be connected to the outer case of the SMA connect while the back electrode will be connected to the needle.

3.3.1 The Lithium Niobate Wafer

In our experiment a 36 degree rotated Y-Cut lithium niobate wafer (Boston Piezo-optics, Bellingham, MA) is used. The wafer is coated with gold on both faces as electrode. The wafer has a 0.187 inch diameter and the thickness is 0.0055 inch (139.7μm). Basically an ultrasound transducer is a resonator. The fundamental frequency, which has an acoustic wavelength that is twice its thickness, takes the largest portion of power. Therefore, the frequency of the transducer is determined by the thickness of the piezoelectric material. The frequency of our crystal is around 27 MHz.

3.3.2 Acoustic Impedance and Matching Layer

Molecules or atoms are bond to each other elastically in material. The pressure cause by the compression and expansion of the material is the driving force for acoustic wave to propagate. To describe this acoustic property of material, the characteristic acoustic impedance is defined as the product of its density and acoustic velocity.

$$Z = \rho V$$

Here ρ represents the density of the material, V represents the acoustic velocity.

The acoustic impedance is important because it determines the acoustic transmission and reflection coefficient at the boundary of two materials. For example, Z_1 and Z_2 are the acoustic impedance of two different material 1 and 2. If an acoustic wave coming from material 1 is incident on the boundary, suppose Z_1 and Z_2 are different, then there will be reflection on the boundary. And the reflection coefficient is described as

$$R = \left(\frac{Z_2 - Z_1}{Z_2 + Z_1}\right)^2$$

If Z_1=1, Z_2=1.5, then 4% of the energy will get reflected on the interface.

Generally, in ultrasound experiment, the transducer and the object will be placed in water. There are two reasons: on one hand, ultrasound transducers cannot be placed in air because the sound wave will decay very fast due to its high absorption coefficient in air; on the other hand, ultrasound transducers are mainly used in clinical applications, where human body is the object. And a very large portion of human body is water. So an underwater ultrasound experiment will get the most similar result as in human body. From Table 1 we can see that the acoustic impedance of lithium niobate is $34MRayl$. However, water has an acoustic impedance of $1.5MRayl$. There is a very large impedance mismatch here. The reflection coefficient when sound wave propagate through the interface will be

$$R = \left(\frac{1.5 - 34}{1.5 + 34}\right)^2 = 0.838$$

So 83.8% of the power will be reflected while only a small portion will be transmitted through. Obviously this will largely lower the efficiency of the transducer.

Therefore, in order to get as much energy out of the transducer as possible, a matching layer is placed between the lithium niobate crystal and the medium which is water here. This acoustic matching layer shares the same mechanism with the anti-reflection layer in optics. The matching layer should have a thickness which is a quarter of the desired wavelength. This thickness will ensure that the reflected wave within the matching layer in phase when they exit the layer. From the Krimhotz, Leedom, and Matthaei (KLM) equivalent circuit model, we can the acoustic impedance of the matching layer Z_m is [22]:

$$Z_m = (Z_1 Z_2^2)^{1/3}$$

Z_1 is the impedance of the piezoelectric element and Z_2 is the impedance of the medium. So here

$$Z_m = (34 \times 1.5^2)^{1/3} = 4.245\ MRayl$$

We need to find an electrical conductive material that has acoustic impedance 4.245 $MRayl$ as the matching layer. In the end, a lossy conductive epoxy E-SOLDER 3022 (Von Roll Isola Inc., New Haven, CT) is used as matching layer. The density of E-SOLDER 3022 is $\rho_{3022} = 2.424\ g/cm^3$, the acoustic velocity in E-SOLDER 3022 is $V_{3022} = 1970\ m/s$. Therefore the acoustic impedance of 3022 is

$$Z_{3022} = \rho_{3022} V_{3022} = 4.775\ MRayl$$

Though there is a small difference between the matching layer impedance and the impedance of the epoxy, we still decide to use E-SOLDER 3022 since it is the most suitable material we found and it is very easy to handle.

3.3.3 Acoustic Backing Layer

Backing layer is needed in transducer because it supports the piezoelectric crystal. Also, it has a large influence on the damping characteristic of a transducer. The most effective damping happens when the impedance of the backing layer is similar to that of the piezoelectric crystal. Such a transducer will have a higher sensitivity due to wide bandwidth. When the mismatch between piezoelectric material and the backing layer increases, the sensitivity of the transducer will be reduced while the material penetration increases.

In our experiment, we still use E-SOLDER 3022 as the backing layer because it is acoustically lossy. The loss for E-SOLDER 3022 is 40dB/mm [23].

3.4 Fabrication of Acoustic Stack

The acoustic stack, which includes the lithium niobate crystal, matching layer and backing layer, is the core part of ultrasound transducer.

The matching layer is made first. As we mentioned above, the material for matching layer is chosen to be the conductive epoxy E-SOLDER 3022. It comes with two parts: 3022 resin and NO. 18 hardener. Mix the 3022 resin and the hardener in 100:8 ratio by weight, and carefully apply it on one surface of the lithium niobate

wafer. Since the thickness of the wafer is only 139.7μm, any 3022 mixure residual on the edge will connect the two faces of wafer, shortening the circuit. So we have to be extremely careful here. After the 3022 mixture is applied, we will let it sit for 24 hours in room temperature for curing. Then, an ultrapol End & Edge polisher is used to lapping down the matching layer to its desired thickness, which is a quarter of the acoustic wavelength. A bubble level is used to make sure the sample is parallel with the lapping film. This is vital for the uniformity of the matching layer. Also, a coarse-to-fine process is performed here. First, we use 9 μm particle size lapping films to lapping down the matching layer fast. Then, a 1 μm particle size lapping film is used to precisely control the thickness of the matching layer. Wax is used to attach the lithium niobate wafer to the holder. The thickness of the matching layer is measured by micrometer.

(a) (b)

Figure 3.3 (a) The ultrapol End & Edge polisher. The green color round film is the lapping film. Lithium niobate wafer is attached to the holder which is right above the lapping film. Water dribbles from the black tube is used to cool the contact area. (b) The silver color round wafer. Silver color comes from the 3022 mixture. Wax is used to attach the wafer to the holder.

Fig. 3.3 shows the lapping machine and the lithium niobate wafer with matching layer when it is attached to the holder. The making of the backing layer is straightforward. We decided to use the 3022 mixture again since it is very lossy. The same recipe is used to make the 3022 mixture. Then the mixture is applied to the back of the wafer to around 2 mm thickness. Still, we have to be extremely careful here to prevent the over-flow. In the end, let the 3022 mixture cool down for 24 hours at room temperature. Fig. 3.4 shows the side view of the finished acoustic stack.

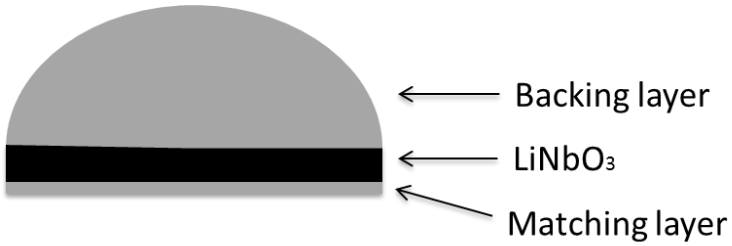

Figure 3.4 The acoustic stack: backing layer, lithium niobate wafer and matching layer.

Again, we need to check the wafer to see if there is any electrical connection between both faces. If there is, use a lapping film to remove these connections due to 3022 mixture overflow.

3.5 Assemble the Lithium Niobate Transducer

After the acoustic stack is finished, we begin to assemble the lithium niobate transducer. The major goal is to build electrical connections to the matching and backing layer. A SMA connector is used here. First, we disassemble a SMA connector, leaving only the outer metal case, the needle and the pin insulator, as shown in Fig.3.5(a) , a brief sketch of side view after it is assembled is shown in Fig.3.5(b) .

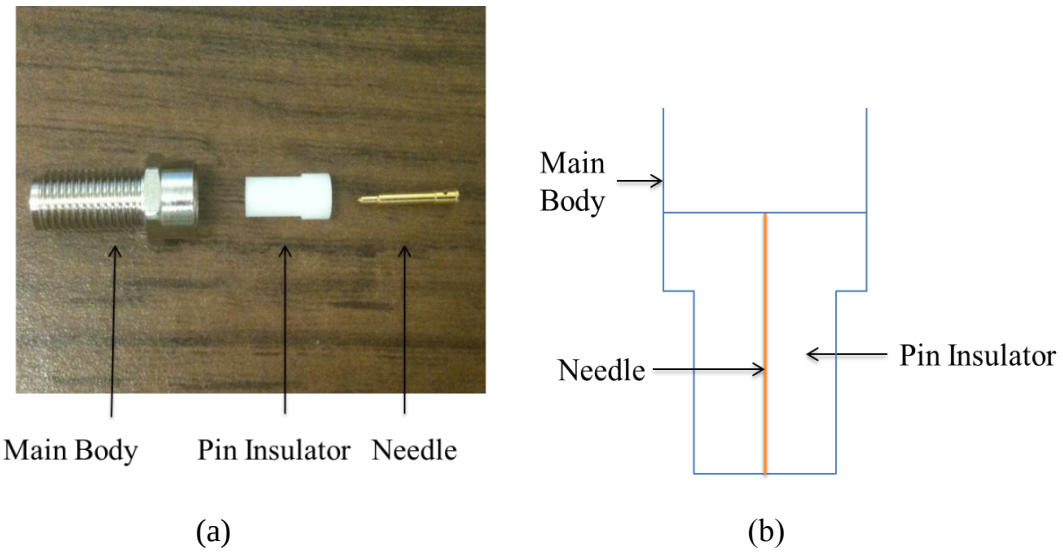

Figure 3.5 (a) The disassembled SMA connector, including main body, the pin insulator and the needle. (b) The side view sketch of SMA after it is assembled.

From the Figure we can see that the end of the needle is very small, which may leads to bad electrical connection. To prevent this, a small piece of metal wire is put into the needle. Then we add some melted solder wire to the metal wire to form a small pillar in order to increase its contact area. These two steps are shown in Fig. 3.6.

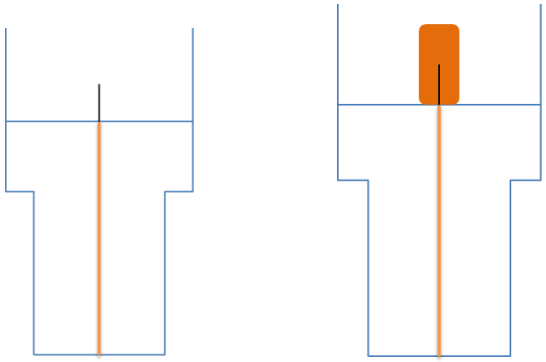

(a) (b)

Figure 3.6 (a) Small metal wires are put into needle. (b) More melted solder wire is added around the metal wire.

Then, a shrink wrap is used to mount on the metal pillar. The shrink wrap is carefully trimmed so it is slightly longer than the metal pillar but lower than the outer case. Then, a non-conductive epoxy named insulcast 501 (American Safety Technologies, Roseland, NJ) is cast into the gap between the outer case and the shrink

wrap. Due to the block of the shrink wrap, this nonconductive epoxy will not flow into the center, which is used for electrical connection. After the insulcast 501 is cured, it is used to support the acoustic stack. These two steps are shown in Fig. 3.7. Also, a picture is taken here in this step.

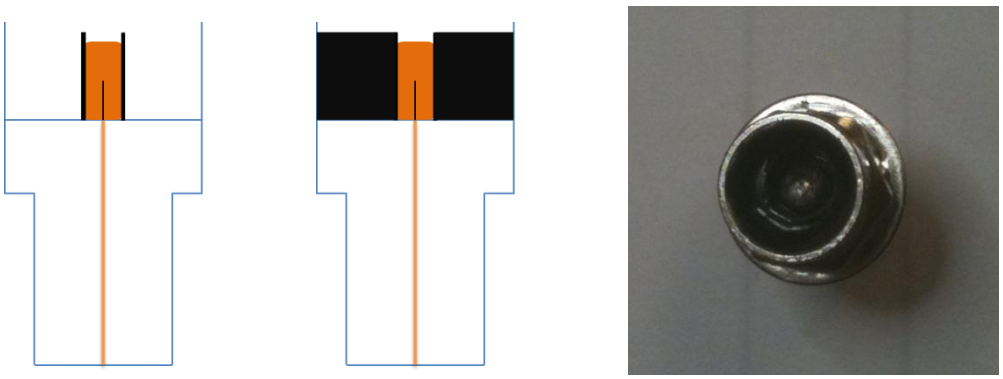

(a) (b) (c)

Figure 3.7 (a) Shrink wrap is mounted on the metal pillar. (b) Insulcast 501 is cast to the gap between outer case and the metal pillar. (c) A picture of the transducer in current stage.

Then, we carefully place the acoustic stack right above the metal pillar. The small concave structure created by the insulcast 501 epoxy will used to support the acoustic stack. A small amount of 3022 mixture is applied between the acoustic stack and the metal pillar to ensure its electrical connection. Then let it sit for another

24 hours for curing. After that, more insulcast 501 is cast into the gap to increase the non-conductive epoxy level to the height of outer case. These steps are shown in Fig. 3.8. Again, a picture is taken to show the transducer in current stage.

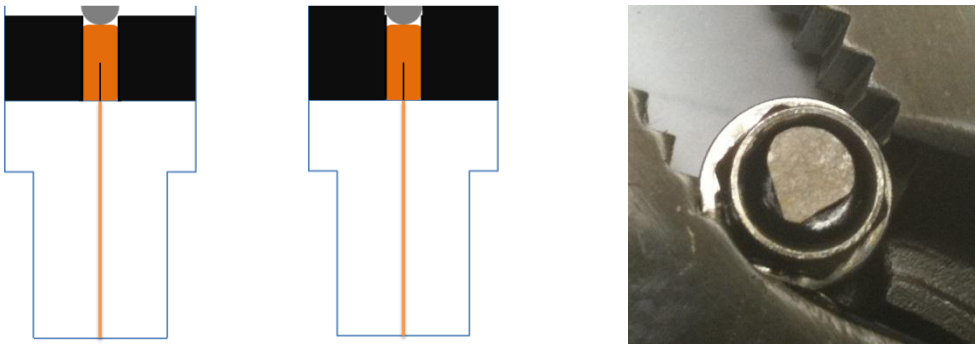

(a) (b) (c)

Figure 3.8 (a) The acoustic stack is placed above the metal pillar. (b) More insulcast 501 is cast into the gap to elevate the non-conductive epoxy level to the height of the outer case. (c) Picture of the transducer after the acoustic stack is placed on metal pillar.

In the final step, a 250 nm layer of gold is coated on the surface of the matching layer using an evaporator. This gold layer is used to connect the matching layer and the outer case. This step is shown in Fig. 3.9(a) and Fig. 3.9(b) is the final product.

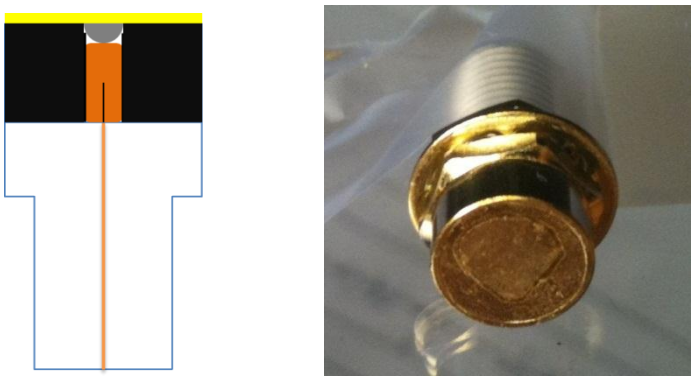

(a) (b)

Figure 3.9 (a) A layer of gold is coated on the matching layer to connect the matching layer with the outer case. (b) The Picture of the final product.

After we assemble the transducer, the conductive matching layer is connected to the outer case of SMA and the backing layer is connected to the needle of SMA. The electrical connection of the transducer is finished in this step.

3.6 Electrical Impedance Matching

The ultrasound transducer has to be connected to a pulser/receiver to generate and receive ultrasound. The cable we use to connect the pulser/receiver is a cable with one BNC connector and one SMA connector. The cable has a characteristic

impedance of 50 ohm. However, the transducer can be seen as a capacitor, which includes a dielectric lithium niobate wafer sandwiched between two gold layers. The capacitor has an imaginary impedance value, which equals to

$$Z_{capacitor} = -j\frac{1}{\omega C}$$

Where ω is the angular frequency, C is the capacitance.

Therefore, if we connect the ultrasound transducer with the cable directly, a very large electrical impedance mismatch will present. This means that large portion of the power will be reflected back at the interface between the transducer and the cable, then the transducer will only be able to generate weak ultrasound signal. So the electrical impedance matching is necessary here.

Although the ultrasound transducer can be seen as a capacitor, there is still resistance exists in the transducer due to the gold layer, matching layer and the backing layer. So the electrical impedance of the ultrasound transducer should be measured first.

In our experiment, a HP 4195A 500MHz Network/Spectrum Analyzer is used to measure the impedance. With different measurement kit, HP 4195A is suitable for transmission measurement, reflection measurement, spectrum measurement and impedance measurement. After we calibrate the machine and compensate for the cable, we are able to perform the impedance measurement. Fig. 3.10 is the result.

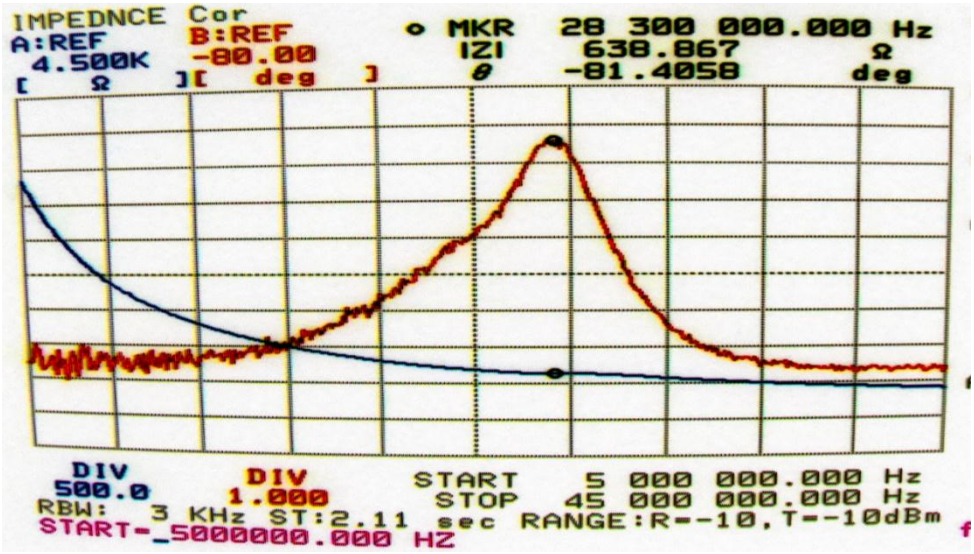

Figure 3.10 The impedance of the ultrasound transducer

The red line here shows phase and the blue line shows magnitude. We will notice that there is a resonance peak on the phase at around 28.3 MHz. Usually the electrical resonance is related to the mechanical resonance of the piezoelectric wafer, which is also the frequency of the ultrasound. Therefore, we can predict that the peak frequency of this ultrasound transducer is around 28.3 MHz. At this frequency, the impedance is

$$Z_{transducer} = 638.867 \times \cos(-81.4) + j \times 638.867 \times \sin(-81.4)$$
$$= 95.53 - \mathrm{j} \cdot 631.68$$

Next, we need to find out the suitable inductor to cancel out the capacitance. This inductor should have an impedance of $\mathrm{j} \cdot 631.68$ at 28.3 MHz. The equation for the impedance of an inductor is

$$Z_{inductor} = j\omega L$$

In order to get the inductance L,

$$\mathrm{L} = \frac{Z_{inductor}}{j\omega} = \frac{Z_{inductor}}{j2\pi f} = \frac{\mathrm{j} \cdot 631.68}{j2\pi \cdot 28.3 \cdot 10^6} = 3.55\ \mu H$$

So an inductor of $3.55\ \mu H$ will be put in series with the transducer to cancel out the imaginary impedance. As for the real part of the impedance, a transformer should be used to change its value from 95.53 ohm to 50 ohm to match the characteristic impedance of the cable. However, for our transducer we didn't add this transformer.

3.7 The Pulse Echo Signal

Fig 3.11 shows the pulse echo signal of the lithium niobate transducer in series with the $3.55\ \mu H$ inductor. The pulse signal is good, but each pulse has 8 cycles, which means that the sound wave is "trapped" in the lithium niobate wafer. One possible explanation is the matching layer is not properly built so the sound wave will get reflected on the interface. Fig. 3.11 shows the pulse echo signal and its spectrum. The -6dB bandwidth is around 15 MHz.

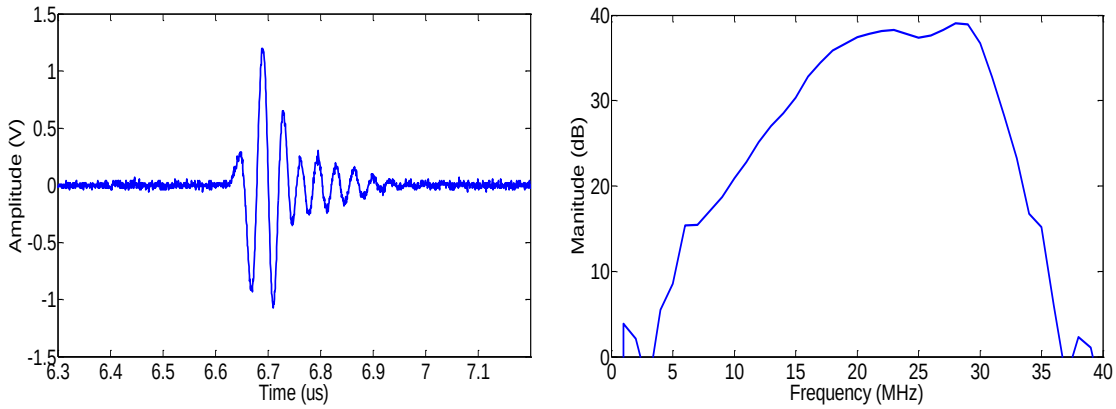

Figure 3.11 (a) Pulse echo signal of the lithium niobate transducer in series with an $3.55\ \mu H$ **inductor. (b) Spectrum of the pulse echo signal.**

3.8 Insertion Loss

The insertion loss characterize the sensitivity of a transducer, the definition is

$$I_L[dB] = 20log\frac{V_{pp\ echo}}{V_{pp\ emitted}}$$

The way to measure the insertion loss is simple: The ultrasound transducer emits a pulse. The pulse travels in the medium, which is water in our experiment, get reflected from a plane perpendicular target. And the echo is received by the same transducer. The target and the medium should have a large acoustic impedance mismatch, which is to ensure that most of the sound wave gets reflected. We use aluminum target which has an acoustic impedance of 17 $MRayl$.

A pulser-receiver (Olympus Panametrics, 5072 PR) is used to generate ultrasound. The peak to peak value of emitted pulse is 91.06 V; the peak to peak value of echo is 3.08 V. However, considering the absorption of water and partially reflected wave due to the interface, the actual emitted pulse is only 74.02 V. Therefore, the insertion loss is

$$I_L[dB] = 20log\frac{V_{pp\ echo}}{V_{pp\ emitted}} = -27.6\ dB$$

A good ultrasound transducer usually has insertion loss around -20 dB, so there is still a lot of room to improve our transducer.

Chapter 4

ULTRASOUND TRANSDUCER WITH ETALON DETECTION

We have built the etalon detector and lithium niobate transmitter separately, now we need to combine these two to make an ultrasound transducer. We have finished the design, however, due to time limitation, we haven't finished the fabrication, and this is our work in the future.

4.1 Basic Structure

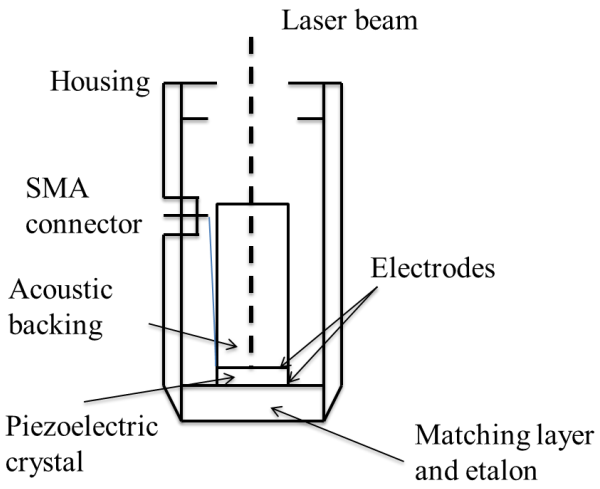

Figure 4.1 Basic structure of ultrasound transducer using optoacoustic detection

The basic structure is similar to the lithium niobate transducer, as shown in Fig. 4.1. The core part is the acoustic stack consists of acoustic backing, piezoelectric crystal and matching layer. It is possible that the etalon itself can be used as matching layer, or we can use polymethyl methacrylate (PMMA) since it is transparent and has proper acoustic impedance. The laser beam will be focused on the etalon; the reflected light will be received by photodetector which is connected to a computer to acquire data. The electrodes are connected to a SMA connected which is embedded on the housing of the transducer for electrical connection.

4.2 The Transparent Backing Layer

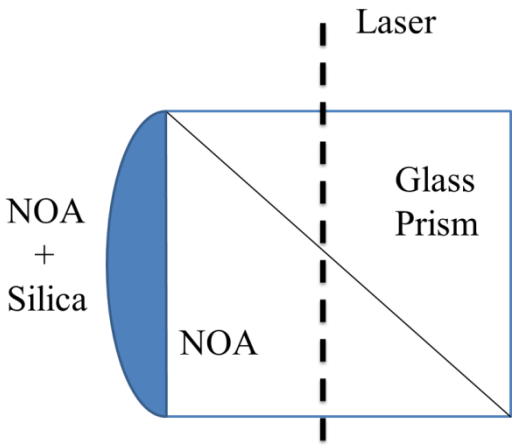

Figure 4.2 The structure of transparent backing layer

As shown in Fig. 4.2, the backing layer consists of three parts: a glass prism, a prism made of NOA (Norland Optical Adhesive), and a layer made of NOA and silica powder. The glass prism and the NOA prism will form a cube where the laser beam passes by. Because the refractive index of glass and NOA are very close. The laser will see only a small reflection. However, the acoustic impedance of NOA and glass differs largely; the acoustic wave will be strongly reflected on the interface. Then the sound wave will decay very fast in the layer made of NOA and silica. Therefore the backing layer is optically transparent and acoustically opaque.

4.3 The Transparent Electrode

Obviously, the acoustic stack should be all transparent except the possible etalon matching layer. Therefore we cannot use gold as electrode anymore. Indium tin oxide (ITO), on the other hand, is a transparent and colorless conductive material. And ITO coating is a mature technology widely used in nowadays. In our experiment, a 200 nm thick ITO layer will be coated on both faces of lithium niobate crystal using sputtering method. Then a metal wire is attached to a small portion of the ITO surface using conductive epoxy. In the end, this metal wire is connected to the SMA connector for electrical connection.

Chapter 5

CONCLUSION

In this paper, we propose an approach to build high frequency ultrasound transducer for real time ultrasound biomicroscopy. The receiving part and the transmitting part are investigated separately.

For the receiving part, an etalon is designed, fabricated and tested for ultrasound detection. An etalon model, in which the thickness of the gold layer is taken into account, is developed and demonstrated. 45 nm is chosen as the optimal gold thickness, providing high reflection while maintaining low loss. Three different material, polystyrene microsphere, SU-8 2005 photoresist and parylene, are used as the transparent layer in etalon. Each one is characterized for its optical property and ultrasound property. Parylene etalon is more suitable for parallel detection due to its more precise thickness control and wider bandwidth. In the end, etalon arrays are fabricated and demonstrated to have similar property as ordinary etalon.

For the transmitting part, lithium niobate crystal is used since it is a piezoelectric material and also transparent. E-SOLDER 3022 is used as the material for matching and backing layer due to its electrical conductivity and proper acoustic impedance. Electrical impedance matching is achieved. The -6 dB bandwidth is measured to be 15 MHz and two-way insertion loss is 27.6 dB.

In the end, we propose an approach to combine these two parts together. A glass prism and a NOA prism is bonded as the backing layer which is optically transparent and acoustically opaque. ITO is chosen as the electrode since it is

electrical conductive and transparent. Etalon or PMMA can be used as the matching layer. Our future work includes building and testing this transparent ultrasound transducer.

REFERENCES

1. National Cancer Institute--National Institutes of Health

2. National Eye Institute-- National Institutes of Health

3. New York Eye and Ear Infirmary, New York, NY

4. F.S.Foster, M.Y.Zhang, Y.Q.Zhou, G.Liu, J.Mehi, E.Cherin, K.A.Harasiewicz, B.G.Starkoski, L.Zan, D.A.Knapik, and S.L.Adamson, "A new ultrasound instrument for in vivo microimaging of mice" Ultrasound Med. Biol. Vol.28 (9), pp. 1165-1172 (2002)

5. J.M. Cannata, J.A.Williams, Q.F.Zhou, T.A.Ritter, and K.K.Shung, "Development of a 35 MHz piezo-composite ultrasound array for medical imaging" IEEE Trans. Ultrason., Ferroelect., Freq. Contr., Vol.53 (1), pp. 224-236 (2006)

6. B. Savord and R. Solomon, "Fully sampled matrix transducer for real time 3D ultrasonic imaging" Proc. IEEE Ultrason. Symp., pp. 945-953 (2003)

7. T. Buma, J.Y. Ye, T.B. Norris, S. Milas, M. Spisar, K. Hollmann, M. O'Donnell, J.D. Hamilton, S. Emelianov, L. Balogh, and J. Baker Jr., "Optoacoustics for biomedical applications", J.Acoust. Soc. Am., Vol 114, No.4, pp. 2377 (2003)

8. Y. Shu, X. Guo, M. Liu, and T. Buma "One-dimensional optoacoustic receive array employing parallel detection and video-rate acquisition", IEEE Ultrasonics Symposium (2010)

9. J.K. Thomson, H.K. Wickramasinghe, and E. A. Ash, "A Fabry-Perot acoustic surface vibration detector-application to acoustic holography," J. Phys. D: Appl. Phys., Vol. 6, pp.677-687 (1973)

10. P. C. Beard and T. N. Mills, "Miniature optical fibre ultrasonic hydrophone using a Fabry-Perot polymer film interferometer," Electron. Lett., Vol. 33, pp. 801-803, (1997)

11. P. C. Beard, A. Hurrell, E. van den Elzen, and T. N. Mills, “Comparison of a miniature, ultrasonic, optical fibre hydrophone with PVDF hydrophone technology,” Proc. IEEE Ultrason. Symp., (1998)

12. http://refractiveindex.info/?group=METALS&material=Gold

13. N. D. Denkov, O. D. Velev, P. A. Kralchevsky, I. B. Ivanov, H. Yoshimura, and K. Nagayama, “Mechanism of formation of two-dimensional crystals from latex particles on substrates”, Langmuir, vol. 8, 3183-3190 (1992)

14. L. Landstrom, D. Brodoceanu, K. Piglmayer, and D. Bauerle, “Extraordinary optical transmission through metal-coated colloidal monolayers”, Appl. Phys. A, vol. 84, 373-377 (2006)

15. C. L. Haynes, A. D. McFarland, L. L. Zhao, R. P. Van Duyne, G. C. Schatz, L. Gunnarsson, J. Prikulis, B. Kasemo, and M. Kall, “Nanoparticles Optics: The importance of radiative dipole coupling in two-dimensional nanoparticle arrays” J. Phys. Chem. B., vol. 107, 7337-7342 (2003)

16. Y. Hou, S. W. Huang, S. Ashkenazi, R. Witte, M. O’Donnell, “Thin polymer etalon arrays for high-resolution photoacoustic imaging”, Journal of Biomedical Optics 13(6), 064033 (2008)

17. A. Kosiorek, W. Kandulski, P. Chudzinski, K. Kempa, and M. Giersig, “Shadow nanosphere lithography: Simulation and experiment,” Nano Lett., vol. 4, 1359-1363 (2004)

18. X. Guo, M. Churgin, and T. Buma, “Optoacoustic sensor based on self-assembled polystyrene microsphere”, IEEE Ultrasonics Symposium, pp. 887-890 (2008)

19. G. S. Kino, Acoustic Waves: Devices, Imaging, and Analog Signal Processing. Englewood Cliffs, NJ: Prentice Hall, pp 27-71 (1987)

20. K. K. Shung, J. M. Cannata and Q. F. Zhou, “Piezoelectric materials for high frequency medical imaging applications: A review”Journal of Electroceramics, vol.19, pp 141-147 (2007)

21. J. Cannata, T. A. Ritter, W. H. Chen, R. H. Silverman, K. K. Shung, “Design of efficient, broadband single-element (20-80 MHz) ultrasonic transducer for medical imaging applications”, IEEE Transactions on Ultrasonics, Ferroelectrics, and Frequency control, vol.50, NO.11 (2003)

22. C. S. Desilets, J. D. Fraser, and G. S. Kino, “The design of efficient broad-band piezoelectric transducers” IEEE Trans. Sonics Ultrason., vol. 25, no. 3, pp.115-125 (1978)

23. H. F. Wang, T. Ritter, W. W. Cao, K. K. Shung, “High Frequency Properties of Passive Materials for Ultrasonic Transducers”, IEEE Trans. Ultra., Ferro. and Freq., vol. 48, no.1, pp. 78-84 (2001)